© 2015. Published by The Company of Biologists Ltd | Development (2015) 142, 2213-2225 doi:10.1242/dev.116517

RESEARCH ARTICLE

TECHNIQUES AND RESOURCES

In vitro myelin formation using embryonic stem cells

Bilal E. Kerman[1,*], Hyung Joon Kim[1], Krishnan Padmanabhan[1,2,3], Arianna Mei[1], Shereen Georges[1], Matthew S. Joens[4], James A. J. Fitzpatrick[4], Roberto Jappelli[1], Karen J. Chandross[5], Paul August[6] and Fred H. Gage[1,‡]

ABSTRACT

Myelination in the central nervous system is the process by which oligodendrocytes form myelin sheaths around the axons of neurons. Myelination enables neurons to transmit information more quickly and more efficiently and allows for more complex brain functions; yet, remarkably, the underlying mechanism by which myelination occurs is still not fully understood. A reliable *in vitro* assay is essential to dissect oligodendrocyte and myelin biology. Hence, we developed a protocol to generate myelinating oligodendrocytes from mouse embryonic stem cells and established a myelin formation assay with embryonic stem cell-derived neurons in microfluidic devices. Myelin formation was quantified using a custom semi-automated method that is suitable for larger scale analysis. Finally, early myelination was followed in real time over several days and the results have led us to propose a new model for myelin formation.

KEY WORDS: Embryonic stem cells, Myelin, Oligodendrocyte, Live imaging, Automated quantification

INTRODUCTION

Myelination of axons by oligodendrocytes in the central nervous system (CNS) and by Schwann cells (SCs) in the peripheral nervous system is crucial for neuronal function and survival. In the absence of myelin, not only is nerve impulse transduction slower but also axons are vulnerable to atrophy and functional deficits due to a lack of trophic support from oligodendrocytes (Nave, 2010). Dysmyelination or demyelination (improper development or loss of myelin, respectively) occurs in many neurological disorders, such as multiple sclerosis (MS), Pelizaeus–Merzbacher disease (PMD) and other leukodystrophies, and as a consequence of spinal cord injury, leading to disruption of electrical impulse conductivity, atrophy of neurons and permanent functional deficits (Miron et al., 2011; Nave, 2010; Peru et al., 2008; Siegel, 2006). Additionally, these symptoms are aggravated by inadequate myelin repair. Therefore, transplantation of exogenous cells and mobilization and recruitment of endogenous cells have been proposed as therapeutic approaches to restore myelin (Cummings et al., 2005; Gupta et al., 2012; Miron et al., 2011; Peru et al., 2008; Potter et al., 2011; Tsuji et al., 2010). For successful outcomes, it is essential to establish and maintain both stimulating and permissive cues for myelination. Such environments can be uncovered through a better understanding of basic oligodendrocyte and myelin biology and by recognizing the molecules that control the myelination process. Consequently, the development of a robust, reliable, easy to modify and quantitative myelination assay is crucial for a deeper study of myelination and to refine or discover therapies for remyelination.

Currently, the myelination process has mostly been studied *in vitro* with isolated primary cells and in postmortem tissues or *in vivo* with animal models (Chen et al., 2010; Dean et al., 2011; Pouya et al., 2011; Watkins et al., 2008). Most of these approaches are restricted by the limited number of cells and animals available and by variability among individual animals, making large-scale experiments difficult. Furthermore, owing to light scattering of the tissues and restrictions on the time of imaging in live animals, observing myelin formation *in vivo* is not currently practical. Efforts to uncouple axons and oligodendrocytes by co-culturing rat-derived primary oligodendrocytes with nanofibers have been made (Lee et al., 2012), but this system has not yet been used with other sources of oligodendrocytes or to study the dynamic process of myelination. By contrast, stem cell technology offers many benefits to overcome the limitations of existing assays. Embryonic stem cells (ESCs) can be readily expanded to a relatively uniform population comprising a large number of cells. The uniformity of cells minimizes experiment-to-experiment differences and studies can be as large or as small as required because ESCs can be readily stored, expanded and transferred between facilities. However, achieving consistent *in vitro* myelination with these cells has been challenging (Brüstle et al., 1999; Jiang et al., 2010; Liu et al., 2000). To develop a consistent and robust *in vitro* myelin formation assay using ESCs, we developed a protocol to differentiate mouse ESCs into myelinating oligodendrocytes. Subsequently, we adapted an existing protocol to generate cortical neurons from mouse ESCs (Gaspard et al., 2009) and established myelin-forming co-cultures. We confirmed functional interaction between neurons and oligodendrocytes and the existence of compact myelin by immunostaining with markers, such as myelin basic protein (MBP) and contactin-associated protein (CASPR; CNTNAP1 – Mouse Genome Informatics), and by transmission electron microscopy (TEM) analysis.

When our co-culture system was grown on conventional cell culture dishes, the effective evaluation of myelin formation was difficult due to the presence of neuronal cell bodies and the random distribution of neurites and myelin within the tissue culture plate. To overcome these limitations, we combined our myelinating co-culture system with microfluidic technology (Taylor et al., 2005). The compartmentalization of oligodendrocytes into a defined region with axons and away from neuronal cell bodies allowed for the direct study of axon-oligodendroglia interactions

[1]Laboratory of Genetics, The Salk Institute for Biological Studies, 10010 North Torrey Pines Road, La Jolla, CA 92037, USA. [2]Computational Neuroscience Laboratory, The Salk Institute for Biological Studies, 10010 North Torrey Pines Road, La Jolla, CA 92037, USA. [3]Crick Jacobs Center for Theoretical and Computational Biology, The Salk Institute for Biological Studies, 10010 North Torrey Pines Road, La Jolla, CA 92037, USA. [4]Waitt Advanced Biophotonics Center, Salk Institute for Biological Studies, 10010 North Torrey Pines Road, La Jolla, CA 92037, USA. [5]Sanofi US, R&D, Genzyme MS/Neurology, 55 Corporate Drive, Bridgewater, NJ 08807, USA. [6]Sanofi US, R&D, Early to Candidate Unit, Tucson Innovation Center, 2090 E. Innovation Park Drive, Tucson, AZ 85755, USA.
*Present address: Research Center for Regenerative and Restorative Medicine (REMER), Istanbul Medipol University, Kavacık Mah. Ekinciler Cad. No.19 Beykoz 34810 Istanbul, Turkey.

‡Author for correspondence (gage@salk.edu)

Received 11 August 2014; Accepted 21 April 2015

Development (2015) 142, 2213-2225 doi:10.1242/dev.116517

and myelin formation in the 'myelination compartment'. With the ability to observe the entire experimental area, we developed a custom semi-automated computer platform, termed computer-assisted evaluation of myelin formation (CEM), to quantify myelin formation. Using CEM, we were able to identify and quantify myelin formation events over a large area with minimal human intervention. In addition to these strengths, our assay is especially suitable for long-term live imaging of the myelin formation process. Longitudinal live imaging allowed us to track oligodendrocytes as they ensheathed and wrapped axons over several days. Our observations revealed that oligodendrocyte processes anchor to axons before wrapping them. By combining live imaging and confocal analysis with previously published data, we propose a new model for myelin formation, in which oligodendrocyte processes survey their environment, anchor to the bare axon and wrap around the axon before forming overlapping sheets of myelin.

RESULTS

A method for oligodendrocyte differentiation from stem cells

To achieve myelination for our study, a consistent source of myelination-competent oligodendrocytes was required. Previously published protocols yielded variable ratios of oligodendrocyte progenitor cells (OPCs) that produced myelin when transplanted into animals; however, *in vitro*, these protocols either failed to produce myelin, were inefficient, or took several months (Brüstle et al., 1999; Jiang et al., 2010; Liu et al., 2000; Numasawa-Kuroiwa et al., 2014). Therefore, we developed a method to differentiate oligodendrocytes from mouse ESCs. We chose a serum-free approach to minimize the variability that is inherent in different batches of serum and to produce a well-defined differentiation cocktail.

First, we generated neural progenitor cells (NPCs) from mouse ESCs (Fig. 1). NPCs can be expanded as needed or stored for further use. OPCs were induced from NPCs using differentiation medium (Fig. 1; see Materials and Methods for media formulations). At the end of 1 week [day (D) 8], ~70% of the population expressed markers for OPCs and/or oligodendrocytes (Fig. 2A,B; supplementary material Table S1). In the second week, we switched to maturation medium to promote the maturation of OPCs (Fig. 1). By D15, mature oligodendrocytes were generated expressing O4 and MBP and showing mature oligodendrocyte morphology, i.e. extended membrane sheaths and highly branched processes (Fig. 2A; supplementary material Table S1). Only a small percentage of the population consisted of astrocytes (5.08%) or neurons (8.38%), highlighting the specificity of our protocol (Fig. 2B; supplementary material Table S1).

Moreover, we confirmed the enrichment of oligodendrocytes by comparing the expression levels of several genes from our oligodendrocyte cultures with undifferentiated NPCs by quantitative PCR (qPCR) on D8 and D15 (Fig. 2C). Expression levels of all tested OPC and oligodendrocyte marker genes were increased several fold over those of NPCs by the first week (Fig. 2C). On D15, genes expressed in mature oligodendrocytes, such as those encoding MBP, proteolipid protein 1 (PLP) and myelin oligodendrocyte glycoprotein (MOG), were increased several thousand fold (Fig. 2C), which is indicative of a well-defined and highly efficient oligodendrocyte generation protocol that yielded mature oligodendrocytes *in vitro* from mouse ESCs.

SCs originate from neural crest cells and myelinate peripheral nerves (Jessen and Mirsky, 2005). To investigate whether SCs were generated alongside oligodendrocytes, we stained cultures for the SC-specific markers myelin protein zero (P0) and peripheral myelin protein 22 (PMP22). No cells positive for either marker were observed (data not shown). In addition, the expression levels of genes encoding P0, PMP22 and periaxin did not show any significant change in D15 oligodendrocyte cultures compared with undifferentiated NPCs by qPCR (supplementary material Fig. S1). We concluded that there was no SC contamination in cultures.

An ESC-based *in vitro* myelination co-culture system

To mimic myelination in the CNS, we established an *in vitro* myelin formation assay in which both neurons and oligodendrocytes were derived from ESCs. To generate neurons, a previously published protocol that enriches for cortical neurons was used (Gaspard et al., 2009). The cells were plated onto coverslips on D12, as described in the protocol, and neurons were allowed to mature for 10-14 days before adding oligodendrocytes to the neuron culture. Oligodendrocytes that were at the end of the 2-week differentiation protocol (D15) were plated on the neurons, thereby starting the myelin formation co-culture (Fig. 1). The co-cultures were kept in myelination medium to promote myelin formation. Oligodendrocytes formed smooth sheaths around neurites (Fig. 3A) and transverse sections of reconstructed confocal images showed that these tubes fully wrapped the neurites (Fig. 3B), indicating that OPCs generated using our

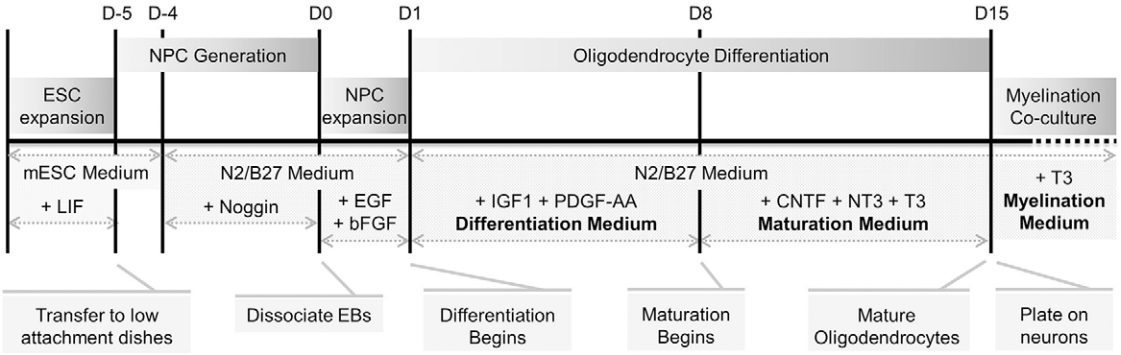

Fig. 1. An overview of the differentiation protocol to generate OPCs and oligodendrocytes from mouse ESCs. Time is given in days (D), with start of NPC expansion as D0 and the start of differentiation as D1. EBs, embryoid bodies; mESC, mouse embryonic stem cell; LIF, leukemia inhibitory factor; EGF, epidermal growth factor; bFGF, fibroblast growth factor basic (FGF2); IGF1, insulin-like growth factor 1; PDGF-AA, platelet-derived grow factor-AA; CNTF, ciliary neurotrophic factor; NT3, neurotrophin 3; T3, triiodothyronine.

Development (2015) 142, 2213-2225 doi:10.1242/dev.116517

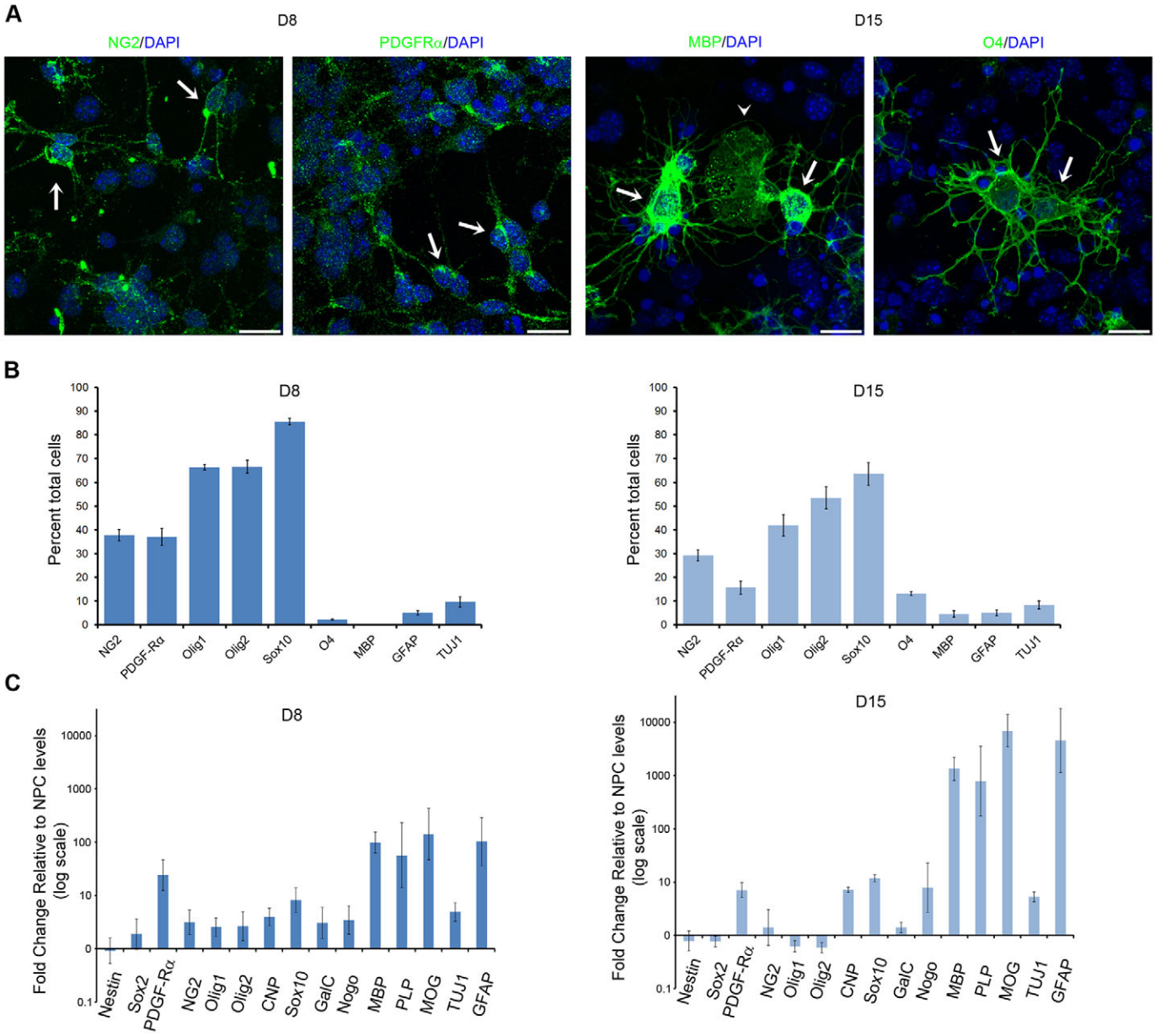

Fig. 2. Evaluation of the differentiation protocol. (A) Representative images of OPCs (arrows in left two panels) and oligodendrocytes (arrows in right two panels) immunostained for the indicated markers (green) and with DAPI (blue) at D8 and D15 of differentiation. Arrowhead marks an extended membrane sheath. (B) Quantification of the number of cells immunostained for several markers of oligodendrocytes, neurons (TUJ1) and astrocytes (GFAP) at D8 and D15 (two independent experiments). (C) Expression analysis of NPC, oligodendrocyte, neuron and astrocyte genes by qPCR at D8 and D15. Fold changes in expression levels compared with undifferentiated NPCs were plotted on a log scale. *Gapdh* expression was used for normalization (three independent experiments). Scale bars: 20 µm.

protocol could mature into MBP-expressing oligodendrocytes that ensheathed and wrapped axons *in vitro*.

Light microscopy can only show if the axons are ensheathed; it cannot confirm whether single or multiple layers of the membrane wrap the axons and if those layers compact to form myelin. To assess the presence of myelin in our co-cultures, we performed TEM analysis and confirmed that the oligodendrocyte membrane wrapped several times around individual axons and formed compact myelin (Fig. 3C). The distance between alternating darker circles (i.e. major dense lines: the electron-dense regions composed of proteins and lipid polar groups) was on average 12.56±0.28 nm (s.d.) (supplementary material Fig. S2), the same as seen in *in vivo* measurements for mammalian CNS myelin (Baumann and Pham-Dinh, 2001; Quarles, 2002). To confirm that oligodendrocytes, but not SCs, wrapped axons, the co-cultures were stained for P0 and PMP22. No cells positive for either marker were observed, confirming the specificity of co-cultures to mimic CNS myelination (data not shown).

CASPR localization shows reciprocal interaction between oligodendrocytes and neurons

During myelination by oligodendrocytes, CASPR initially clusters at the contact sites between axon and oligodendrocyte processes, then spreads across the entire ensheathed portion of the axon and finally accumulates only at the paranodes (Eisenbach et al., 2009; Pedraza et al., 2009). This premyelination CASPR accumulation does not

Development (2015) 142, 2213-2225 doi:10.1242/dev.116517

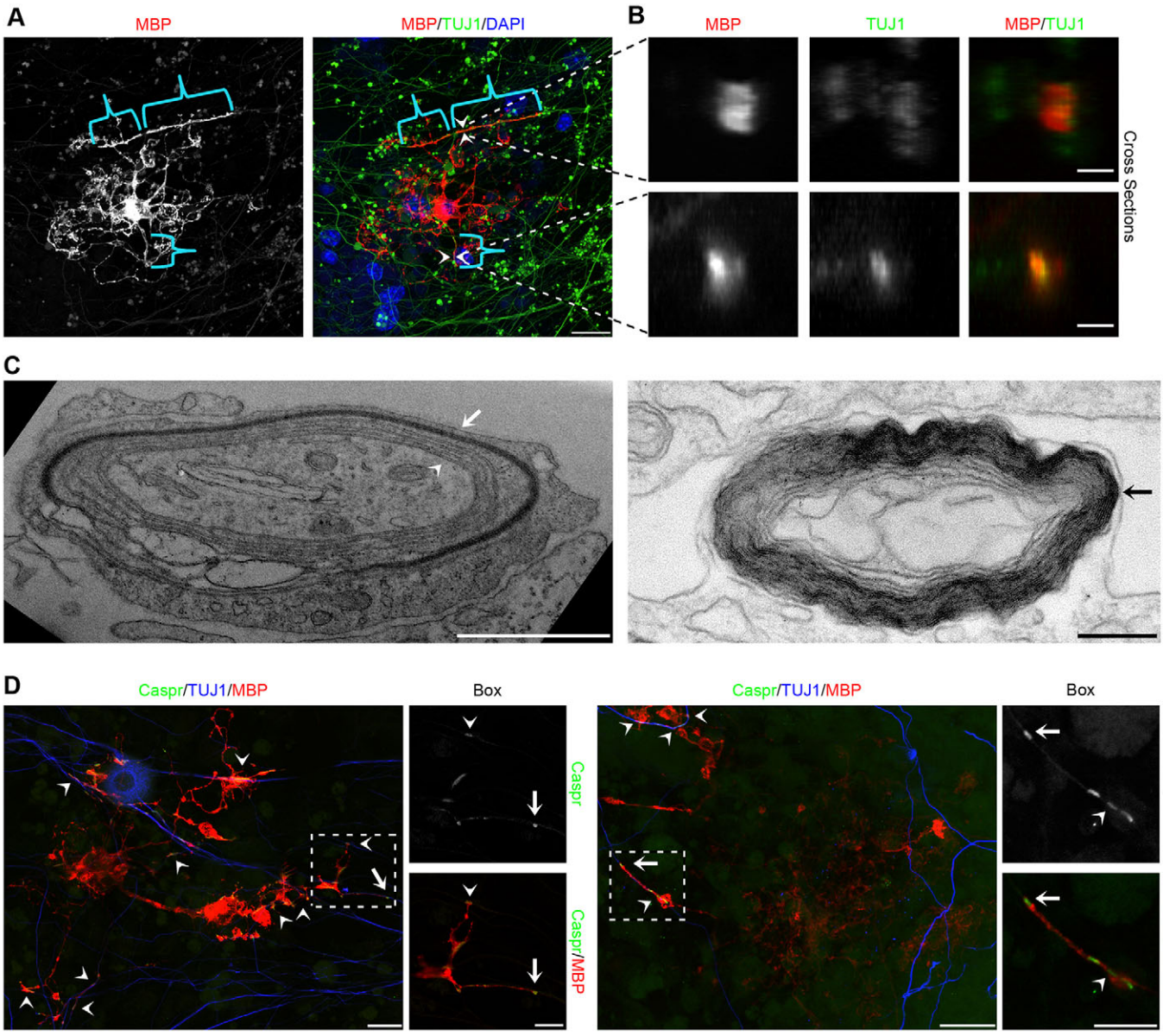

Fig. 3. An *in vitro* co-culture system of myelin formation. (A,B) An example of a myelinating oligodendrocyte in a mixed co-culture. (A) Oligodendrocyte (MBP) only (left), and neurites (TUJ1) and oligodendrocyte (right). Brackets mark regions indicating myelin, i.e. tubes of oligodendrocyte extensions wrapping neurites. (B) Optical transverse sections of oligodendrocyte tubes wrapping neurites at the regions marked with arrowheads in A. (C) TEM images showing compaction of the oligodendrocyte membrane around axons to form myelin (arrows in both panels) as well as part of an oligodendrocyte membrane that has not compacted (arrowhead in the left panel). (D) Two examples of CASPR localization during myelination in mixed co-cultures. CASPR either spread along neurites (arrowheads) or concentrated at portions of neurites (arrows) in contact with oligodendrocyte processes. Boxed regions are shown at higher magnification to the right as projections of the relevant optical *z*-sections. Scale bars: 20 µm in A and in D main panels; 3 µm in B; 1 µm in C left; 200 nm in C right; 10 µm in D higher magnifications.

occur during SC myelination and is characteristic of a reciprocal interaction between oligodendrocytes and neurons. Therefore, we characterized CASPR localization in our co-cultures to assess the functional quality of ESC-derived oligodendrocytes.

CASPR either spread along axons at the regions of contact with oligodendrocytes or densely accumulated at the ends of the region wrapped by oligodendrocytes (Fig. 3D). Thus, similar to primary oligodendrocytes and neurons, ESC-derived oligodendrocytes and neurons interacted reciprocally in myelinating co-cultures. Dual CASPR localization, along both the axons and at the ends of oligodendrocyte wraps, demonstrated that several phases of myelination, including initial contact, ensheathment and compacted myelin, coexisted in our co-cultures. Given that we showed compact myelin formation and that oligodendrocytes interacted with neurons in a functional manner, we concluded that not only did our protocol yield oligodendrocytes that mimicked primary oligodendrocytes but also our co-culture system was representative of biologically relevant myelin formation. Taken together, these results yielded a myelin formation model in an easy-to-manipulate *in vitro* environment.

Adapting the myelinating co-culture system into microfluidic devices

On conventional cell culture platforms, neurons grow and extend neurites in random orientations. Consequently, myelin is distributed

Development (2015) 142, 2213-2225 doi:10.1242/dev.116517

arbitrarily, and quantifying significant numbers of myelination events requires the monitoring of a large portion of the plate. As a next step to optimizing myelin formation co-culture assays, we sought to adapt the system to a platform in which myelination events could be clustered together. Such clustering into a defined area would improve quantitative measurements and also make it easier to track myelination in real time. Previously, primary neurons were cultured in a compartmentalized manner using microfluidics-based neuron culture devices (Taylor et al., 2005), which allowed for the isolation of axons from cell bodies by using microgrooves that interconnected the two main compartments (supplementary material Fig. S3A).

In the conventional microfluidic device design, the capillary forces inside the enclosed compartment of the neuronal compartment only allow 10-20% of ESC-derived neurons to remain in the compartment, which results in a low density of axons growing into the myelination compartment (supplementary material Fig. S3B). To overcome this limitation of low axon density, we introduced a new design that replaced the enclosed compartment with an open well, which restricted almost all of the neurons to the neuronal compartment due to minimized flow (Fig. 4A,B; supplementary material Fig. S3B).

Similar to the experiments in the standard mixed co-cultures, we plated mouse ESC-derived neurons on D12 into the neuronal

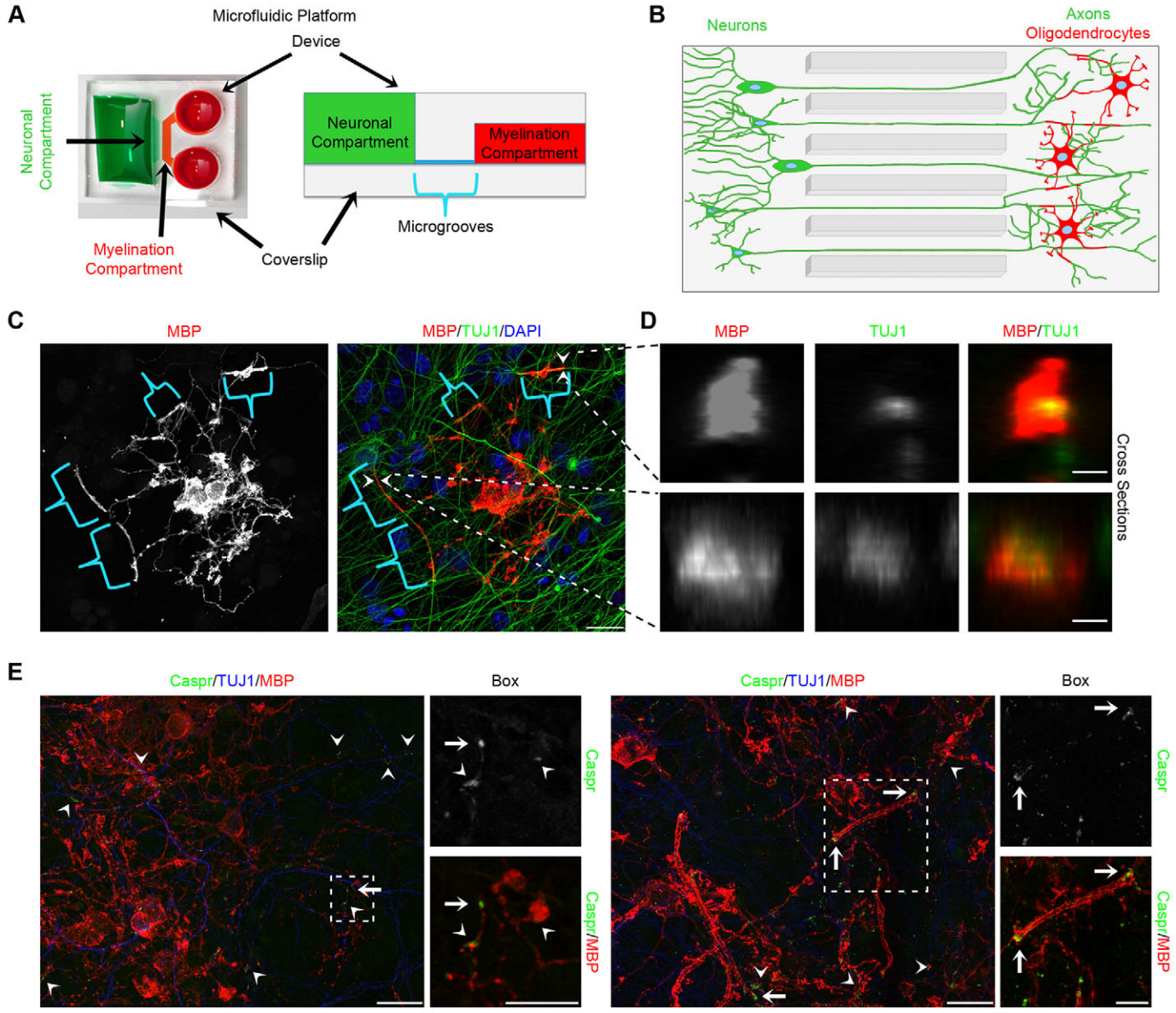

Fig. 4. Myelin formation in microfluidic devices. (A,B) Microfluidic device used for the myelin formation assay. (A) Left, top view; right, schematic cross-section. Neurons were plated into the open neuronal compartment. Oligodendrocytes were plated into the closed myelination compartment. (B) Representation of myelin formation in the microfluidic device. Axons extend through microgrooves into the myelination compartment, where oligodendrocytes ensheathe them. (C,D) An example of a myelinating oligodendrocyte in a microfluidic device. (C) Oligodendrocyte (MBP) only (left), and neurites (TUJ1) and oligodendrocyte (right). Brackets mark regions indicating myelin, i.e. tubes of oligodendrocyte extensions wrapping neurites. (D) Optical transverse sections of oligodendrocyte tubes wrapping neurites at the regions marked with arrowheads in C. (E) Two examples of CASPR localization during myelination in a microfluidic device. Similar to mixed co-cultures, CASPR either spread across neurites (arrowheads) or concentrated at portions of neurites (arrows) in contact with oligodendrocyte processes. Boxed regions are shown at higher magnification to the right as projections of the relevant optical *z*-sections. Scale bars: 20 µm in C; 3 µm in D; 20 µm in E main panels; 10 µm in E higher magnifications.

Development (2015) 142, 2213-2225 doi:10.1242/dev.116517

compartment. In 10-14 days, neurons extended many axons into the myelination compartment (supplementary material Fig. S3B). At this point, D15 oligodendrocytes were plated into the myelination compartment (Fig. 4B). In 2 weeks, oligodendrocytes ensheathed axons, which appeared as elongated tubes (Fig. 4C). Transverse sections of reconstructed confocal images showed complete wrapping of neurites (Fig. 4D).

Next, we examined whether oligodendrocytes and isolated axons in the microfluidic devices would also interact reciprocally to concentrate CASPR. Consistent with our observation in the standard mixed co-culture, CASPR spread along or concentrated on axons (Fig. 4E), which required interaction between oligodendrocytes and axons, demonstrating the presence of several phases of myelin formation from initial contact to compacted myelin in device co-cultures, similar to standard mixed co-cultures.

In summary, we established an *in vitro* myelin formation assay through a combinatorial approach to achieve a compartmentalized co-culture of ESC-derived oligodendrocytes and neurons. This platform provides an ideal method for quantifying myelin formation because the experimental compartment is highly enriched in axons and oligodendrocytes, allowing for more accurate quantitation of myelin formation. Moreover, many myelin formation events can be monitored live by focusing on a relatively small area instead of scanning the entire plate.

Quantification of myelin formation

Although attempts at quantifying myelination events have been made, a number of challenges remain. Counting the number of smooth, tubular-looking segments of oligodendrocyte membrane or manually tracing these segments are two of the main strategies employed (Stancic et al., 2012; Watkins et al., 2008; Yang et al., 2012), but these approaches are often prohibitive when trying to compare several conditions and/or to analyze the entire experimental area due to the large time and manpower requirements. To improve the throughput, automated quantification is the key. Zhang et al. (2011) developed a fluorescence-based method that relies on overlap between mature oligodendrocytes and axons, visualized by MBP and neurofilament, respectively. They showed that a fluorescence-based method could identify factors that affect myelination (Zhang et al., 2011). We took a similar fluorescence-based approach to develop a computer platform (CEM) that could be used broadly. Therefore, CEM was written mainly on ImageJ [see supplementary material Appendix S1 (CEM users guide) and Appendix S2 (CEM package)]. CEM was able to identify and quantify myelin formation within the entire myelination compartment and to detect changes in myelin formation (Fig. 5).

First, the myelination compartment was imaged using confocal microscopy and the entire compartment was reconstructed (~10×1.5 mm^2; Fig. 5A-C; supplementary material Fig. S4A). The algorithm for identification of myelin formation was based on detection of colocalization between neurons and oligodendrocytes after the cell body regions were identified and removed to prevent false positives. To perform calculations, the images were first turned into binary images, i.e. all empty (black) pixels were zero and all pixels with signal were 255 (Fig. 5B,C; supplementary material Fig. S4A). A crucial step in this conversion was to choose a reference slice with a large amount of positive signal and low background noise for optimal thresholding (Padmanabhan et al., 2010). Binary images were further processed to remove cell bodies of oligodendrocytes and neurons, as described in the Materials and Methods (supplementary material Fig. S4B). The overlap between the resulting images was identified as 'myelin' that, by the calculation of the algorithm, encompassed ensheathment as well as compact myelin (Fig. 5D; supplementary material Fig. S4D). Finally, the total amount of 'myelin' was calculated by counting overlapping pixels and the ratio of myelinated axons was calculated by dividing the former value by the total pixel count of neurons (2.61%, n=11; Fig. 5E).

Some experiments might need to be performed on neurons that are subject to different manipulations or conditions because it is not possible to grow them in separate cultures (for example, shRNA treatment will affect only a subset of neurons). Such a scenario was mimicked by expressing GFP in a subset of neurons in our co-cultures. Using the strategy described above, CEM identified the GFP and nonGFP axons and the myelin formation of each subset (supplementary material Fig. S4C,D). As GFP expression alone does not affect myelination, the 'myelin' ratios of each subset were not significantly different (GFP 2.19%, nonGFP 2.78%; P=0.47, n=11; Fig. 5E).

The thyroid hormone triiodothyronine (T3) is known to promote myelination (Barres et al., 1994). 'Myelin' with (+) or without (−) T3 supplementation was quantified to evaluate the capability of CEM to assess myelin formation under different manipulations (Fig. 5F, left two columns). To make the comparison clearer, a myelin quotient (MQ) was calculated by normalizing myelin ratios to an average of +T3 ratios, which was assigned a value of 1. −T3 MQ was significantly lower than +T3 MQ, as expected (0.070 and 1, respectively; P=0.007).

To test if the identified 'myelin' was a random overlap or had biological significance, the joint probability of a pixel being positive for both MBP and TUJ1 (TUBB3 – Mouse Genome Informatics) due entirely to chance was calculated. When this +T3 chance probability was compared with the experimentally calculated probability of a pixel being identified as myelin, it was significantly different (P=0.0025; supplementary material Fig. S4F). We performed the same analysis for the −T3 condition and the experimental value was again significantly higher than chance (P=0.0079; supplementary material Fig. S4F). Next, to test whether changes in MBP expression alone are sufficient to account for the effects under ±T3, we equalized MBP pixel numbers of +T3 to −T3 and compared overlap probabilities. The two values were significantly different (P=0.0192; supplementary material Fig. S4F), suggesting that a reduction in MBP levels alone did not explain the reduced MQ value.

Another advantage of having a normalized MQ was that we could test CEM against manual quantification. Manually calculated +T3 MQ was again assigned a value of 1. −T3 MQ was 0.059, which is significantly lower than the manually calculated +T3 MQ (P=0.012) but not significantly different from the −T3 MQ calculated by CEM (P=0.833; Fig. 5F).

In conclusion, CEM provided a semi-automated and unbiased quantitative approach for evaluating the biology of myelin formation with statistical authority. It was applied to analyze large data sets and was used to evaluate the effects of genetic factors and/or different treatments within a sample, such as GFP versus nonGFP and ±T3, both necessary precursors to expanding our assay into large screens. Moreover, the resulting output of the algorithm contained values for several parameters relevant to myelin formation, allowing flexibility in the analysis (supplementary material Fig. S4E).

We next tested whether it was possible to improve quantification by adding cell-shape recognition. The images were processed through the filament analysis function of Imaris software (Bitplane). Many weaker-stained processes were omitted by the software and several false-positive filaments were drawn connecting bright points

Development (2015) 142, 2213-2225 doi:10.1242/dev.116517

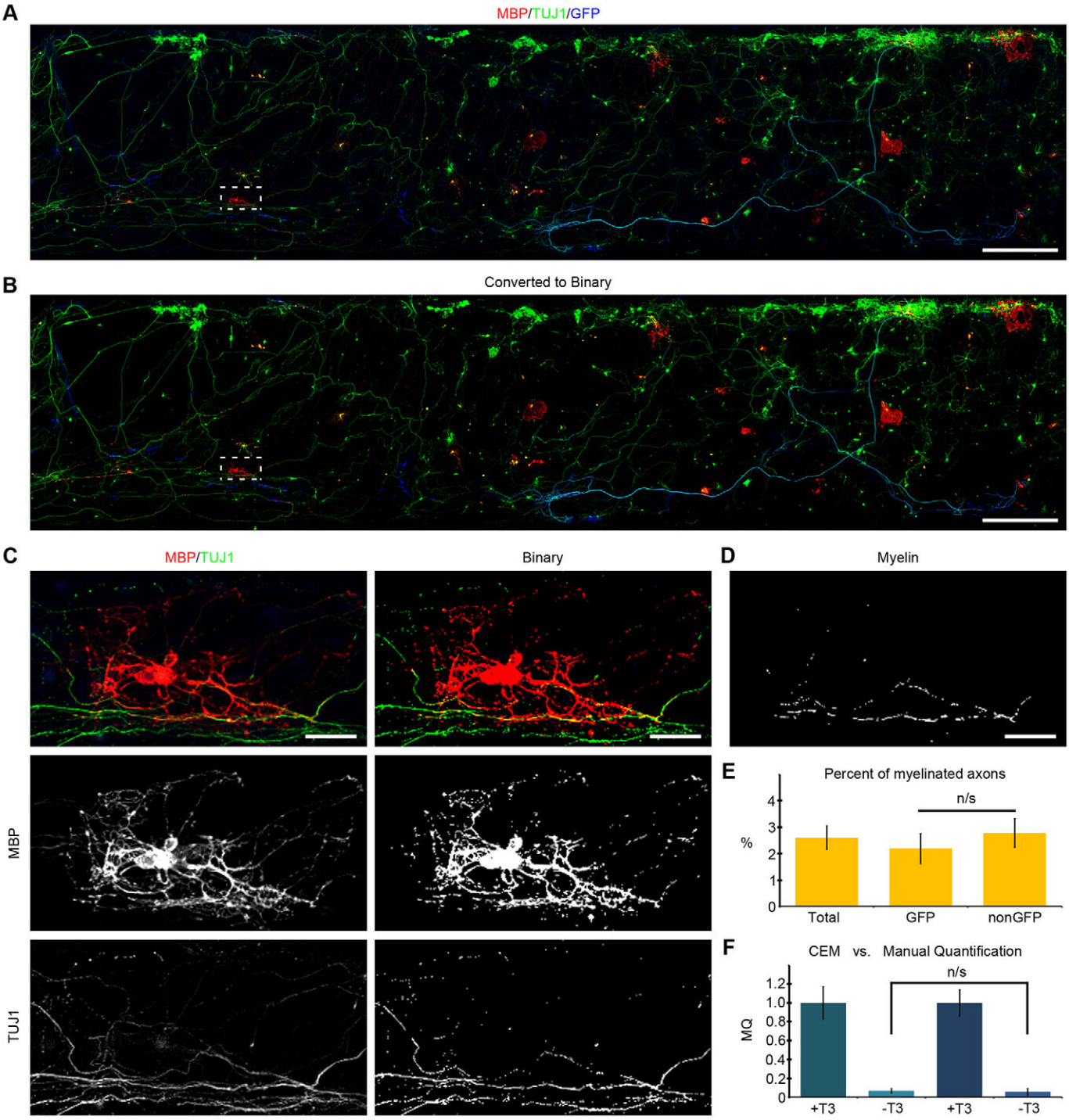

Fig. 5. Quantification of myelin formation. (A) A representative image of the entire myelination compartment at 2 weeks of co-culture. The image is a mosaic of ~100 overlapping stitched tiles and maximum intensity projection of the confocal stacks. Neurons (TUJ1, green), oligodendrocytes (MBP, red) and GFP (blue). (B) The same device after binary conversion. (C) Higher magnification of the boxed regions in A and B. Left, confocal images; right, binary images. (D) Identified myelin in the boxed region. (E) Myelin quantified as a percentage of myelinated neurites among all neurites (total), GFP-expressing neurons (GFP) and neurons not expressing GFP (nonGFP) on 11 devices. (F) Comparison between CEM and manual myelin quantification with or without T3 supplementation (CEM quantification: 11 +T3, 5 –T3 devices; manual quantification: 5 +T3, 5 –T3 devices). MQ, myelin quotient. n/s, not statistically significant (Mann-Whitney *U*-test). See also supplementary material Fig. S4. Scale bars: 500 µm in A,B; 40 µm in C,D.

close to each other (data not shown). Moreover, the processing of each image took almost a day and required a computer with a large amount of RAM (>100 gigabytes), making the strategy not easily accessible. Therefore, cell-shape recognition in its current form is not only significantly failure prone but is also time and resource consuming. When better algorithms for cell-shape recognition are developed, CEM can be updated to take advantage of them.

One limitation of all quantification methods that rely on fluorescent colocalization, including CEM, is that it is impossible to distinguish contact on axon/single wrap versus compact myelin.

Development (2015) 142, 2213-2225 doi:10.1242/dev.116517

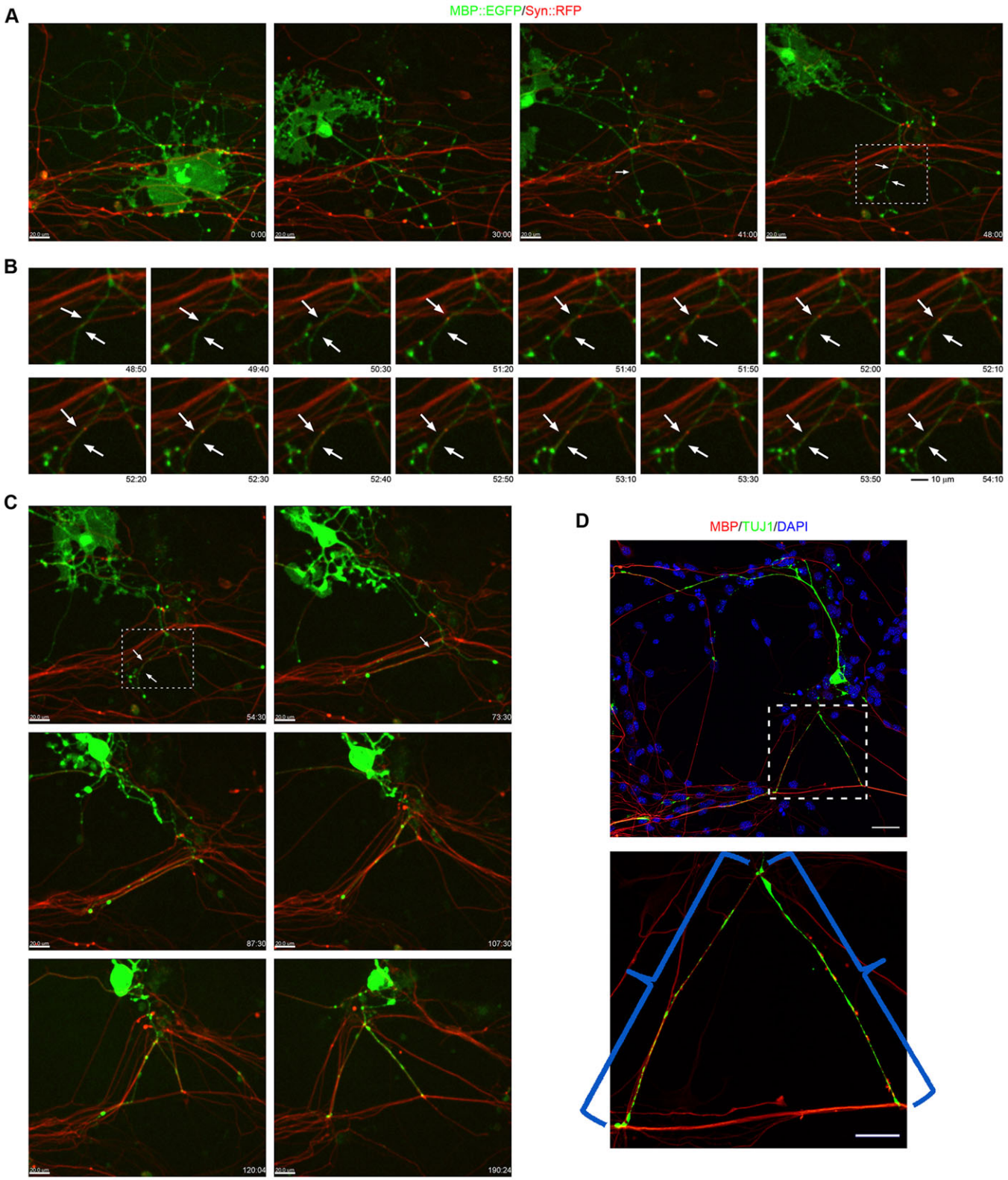

Fig. 6. Live imaging of myelin formation. Selected frames from supplementary material Movie 1 monitoring an oligodendrocyte wrapping a neurite. See also supplementary material Movie 2 and Fig. S5. Arrows point to anchor points and oligodendrocyte processes in the course of wrapping. (A) The oligodendrocyte processes surveyed around and along the axon by constantly moving, extending and retracting before anchoring. (B) The boxed region in A at further time points from 48 h 50 min. The anchored process surveyed further and wrapped the axon (arrows). (C) The boxed region in A at further time points from 54 h 30 min. Wrapping of other neurites continued for at least another 100 h. Note that there was a 54-min gap between 118 h 30 min and 119 h 24 min due to a feeding medium change. (D) The same oligodendrocyte was immunostained after live imaging was complete. Maximum intensity projection of the entire oligodendrocyte (top) and a higher magnification of the boxed region to focus on structures that are reminiscent of helical spiraling (bottom, brackets). Time is shown as hours:minutes. Scale bars: 20 μm in A,C; 10 μm in B; 30 μm in D top; 15 μm in D bottom.

Development (2015) 142, 2213-2225 doi:10.1242/dev.116517

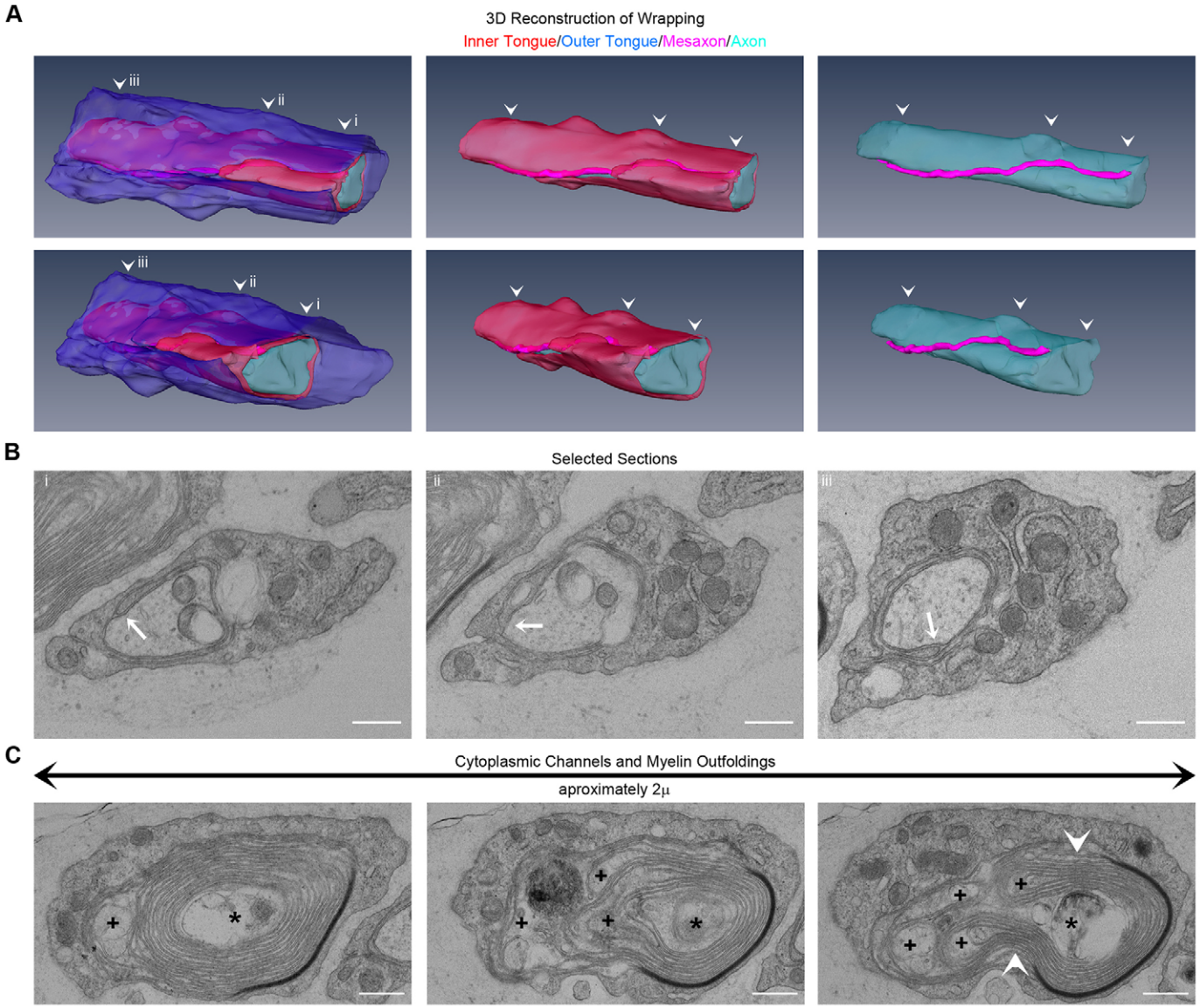

Fig. 7. A 3D reconstruction and selected sections of serial EM sections. (A) Two views of a reconstructed wrapping event. Arrowheads indicate positions of the EM views (i-iii) in B. (B) EM views of selected sections from the serial stack. The axon was wrapped twice for most of the ~5-μm length that was sectioned. The location of the mesaxon (arrow) is compatible with lateral extension of an anchored process. See also supplementary material Movie 3. (C) Sections highlighting complex cytoplasmic channels (+) and myelin outfoldings (arrowheads) that probably arise due to lateral membrane expansion. Asterisk, axon. Scale bars: 400 nm in B; 500 nm in C.

However, given that CEM detected differences in myelination under two conditions comparable to manual quantification and can process several images with minimal human intervention, it is a valuable tool to quantify myelination of large data sets such as drug screens. When necessary, CEM can be followed by a more detailed analysis of selected candidates to quantify compact myelin.

Live imaging reveals a novel mechanism for myelin formation: 'SARAPE'

The final structure of myelin – several wraps of oligodendrocyte membrane around an axon – has been well described through electron microscopy (EM) and light microscopy (Knobler et al., 1976; Remahl and Hildebrand, 1990a,b; Siegel, 2006; Snaidero et al., 2014). However, an understanding of the dynamics of wrapping, especially the initial steps, is still incomplete. Serial section EM analysis of the developing CNS showed non-uniformity in the number of layers of the ensheathing oligodendrocyte process along an axon and bidirectional ensheathment within a developing internode, i.e. the inner ensheathing layer became the outer layer (Knobler et al., 1976; Remahl and Hildebrand, 1990a,b). Based on these observations, it has been proposed that the oligodendrocyte sheath around an axon is initially helical and then elongates and finally undergoes extensive remodeling to reach complete wrapping and compaction. Such helical wrapping is also observed by fluorescent labeling of oligodendrocyte membranes and cytoplasm (Ioannidou et al., 2012). Non-uniformity of wrapping along an internode was also reported in a recent study that combined live imaging and serial block-face imaging (Snaidero et al., 2014).

As a consequence, most of the existing models of myelination predict that the front edge of the oligodendrocyte process continuously grows while wrapping the axon: for example, the 'carpet crawler' model, in which the oligodendrocyte process flattens out and expands

Development (2015) 142, 2213-2225 doi:10.1242/dev.116517

after contact with the axon and then wraps the axon like a rolling carpet (Bauer et al., 2009; Bunge et al., 1989); the 'serpent' model, in which the oligodendrocyte process wraps around the axons in a helical fashion first, like a corkscrew, and then expands into overlapping sheets (Asou et al., 1995; Bauer et al., 2009; Ioannidou et al., 2012; Knobler et al., 1976); and the 'liquid croissant' model, in which the oligodendrocyte process continuously wraps and spreads sideways along the axon (Snaidero et al., 2014; Sobottka et al., 2011). Alternatively, through a detailed analysis of CASPR and NF155 (NFASC – Mouse Genome Informatics) localization during myelination, Pedraza et al. (2009) proposed that the initial contact between the axon and the oligodendrocyte process persists throughout myelination and the membrane wraps the axon like a yo-yo before expanding laterally along the internode; then, the leading edges of all the overlapping layers expand and draw closer at the paranodes.

Part of the controversy about these current models describing the process of myelination is that they were developed primarily through static images and, when available, with the support of relatively short-term live-imaging data sets, which leaves many questions unanswered. To clarify the dynamics of wrapping, in the current study the initiation and progression of myelination were tracked live for up to almost 8 days by visualizing oligodendrocytes and axons using membrane-localized GFP and RFP, respectively (Fig. 6; supplementary material Fig. S5, Movies 1 and 2). Intriguingly, this was a dynamic process in which oligodendrocyte processes performed surveys around and along the axon by constantly moving, extending and retracting as if they were sensing their environment (Fig. 6A). Next, a process attached itself at one or two points on the axon but was otherwise free and continued to survey, a step we termed anchoring. After a period of time that varied from process to process, the oligodendrocyte membrane wrapped the axon by folding repeatedly around it (Fig. 6B). The processes were relatively stable for ~20 h, suggesting that the initial wrapping of the axon was complete (Fig. 6C). In a consecutive analysis, we stopped live imaging and imaged the same oligodendrocyte at higher resolution after immunostaining (Fig. 6D). The processes that we observed anchored and wrapped around the axon were reminiscent of previously observed helical spiraling (Ioannidou et al., 2012). Based on live-imaging data, it does not seem plausible that the process crawled around axons like a snake, forming a perfect corkscrew-like structure, as was previously suggested in the variants of the serpent model, because the process was anchored on the axon before wrapping, as was also proposed by Pedraza et al. (2009).

To assess the wrapping process at the ultrastructural level, we performed 3D EM analysis by serial section EM using an ATLAS scanning approach (Hayworth et al., 2006). The inner and outer tongues (the inner and outer layers wrapping the axon) and the mesaxon (tip of the inner tongue) were identified on an axon that was wrapped twice (Fig. 7; supplementary material Movie 3). Strikingly, the mesaxon wound around the axon as would be expected if the oligodendrocyte process wrapped around the axon and started expanding laterally (Fig. 7A,B). Such lateral expansion would push the leading edges of the membrane sheets towards future paranodes, as was proposed by Pedraza et al. (2009) and observed recently by Snaidero et al. (2014) through live imaging of late stage myelination and serial EM. Consistently, we also observed cytoplasmic channels in the form of myelin outfoldings that facilitate membrane delivery to the growing leading edges (Fig. 7C). Hence, after the initial anchorage and wrapping of the process around the axon, myelination should continue by lateral expansion of the ensheathed layers.

Thus, we propose a mechanism to unify our data concerning early wrapping dynamics with our observations and those of others on later stages of myelination, including: (1) anchorage, wherein an oligodendrocyte process first surveys the environment and the axon in a dynamic fashion and then anchors on the axon while continuing to survey; (2) the unanchored part of the process folds over and wraps the axon; and (3) the process expands along the axon as flattened membrane sheaths that slip over each other to form many layers, the leading edges of which eventually meet at the paranodes (Fig. 8; supplementary material Movie 4). We call this mechanism SARAPE (survey, anchor, wrap and expand) – a term derived from the Mexican blanket-like shawl.

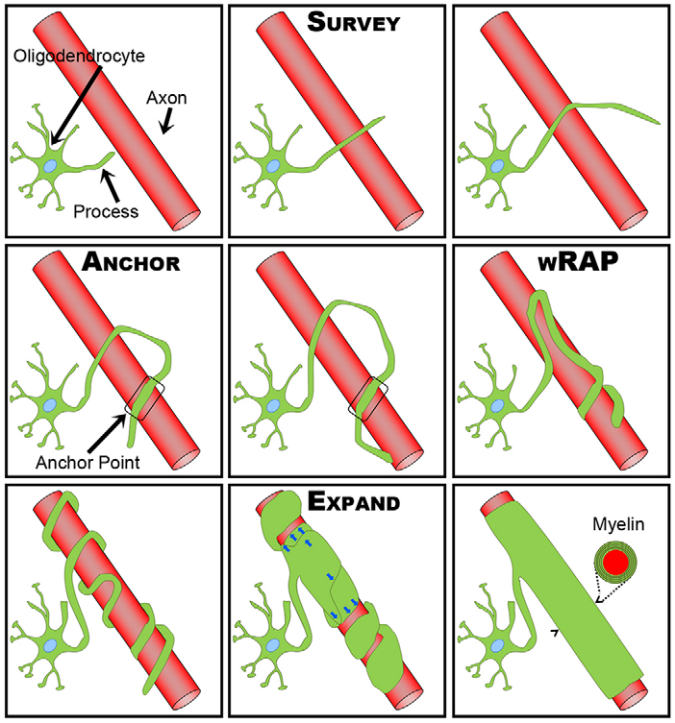

Fig. 8. The SARAPE model of myelination. SARAPE (an acronym for survey, anchor, wrap, expand) describes the oligodendrocyte as it first surveys its environment, anchors on the axon and wraps it. Finally, the oligodendrocyte membrane expands (blue arrows) to cover the axon. See also supplementary material Movie 4.

DISCUSSION

The process and mechanism of myelination in the CNS are still poorly understood. We set out to establish an efficient and reliable assay to study this process. First, we developed a protocol to differentiate myelination-capable oligodendrocytes from mouse ESCs and assessed their identity and maturation levels by both immunostaining and qPCR. When co-cultured with ESC-derived neurons, these oligodendrocytes reproducibly formed compact myelin. We adapted this co-culture system as a myelin formation assay to an optimally engineered microfluidic device, thereby establishing an assay that is robust, reliable, easy to modify and quantitative. Introduction of a semi-automated myelin evaluator, CEM, made it feasible to quantify large data sets such as the entire experimental area, i.e. the myelination compartment, circumventing any sampling bias.

With the advancement of induced pluripotent stem cell (iPSC) technology, an increasing number of neurological diseases are being modeled *in vitro*. Recently, myelin pathology of PMD has been replicated using patient-derived iPSCs (Numasawa-Kuroiwa et al., 2014). iPSCs from MS patients are also available (Douvaras et al., 2014; Song et al., 2012). It is possible to adapt these models to the

Development (2015) 142, 2213-2225 doi:10.1242/dev.116517

microfluidic co-culture environment to study myelination. CEM can identify and quantify myelin on images from any myelinating platform, making the results and framework presented here practical to apply to a number of different systems, ranging from iPSC to animal models of neurological diseases.

Finally, we used this myelin formation assay to image the myelination process in real time, following oligodendrocytes over several days as they surveyed around and along axons by constantly extending and retracting their processes. It is possible that this surveying activity allows oligodendrocytes to identify axons that carry the correct signals to be myelinated. Surprisingly, we observed that the process anchored on the axon but continued to survey. This observation is consistent with earlier work by Asou et al. (1995), although that work was conducted at much lower resolution and for a shorter time period. Additionally, it has been suggested that the interaction between CASPR and its binding partner on the glial membrane, NF155, is never broken from the initial contact to completion of myelination (Pedraza et al., 2009). Therefore, it is possible that these proteins are part of the anchor. Further studies are required to explain the nature of the anchor point and the details of the interactions between oligodendrocytes and axons. It will also be intriguing to examine through additional studies whether myelination occurs through SARAPE *in vivo* in mouse and in other organisms.

We developed an ESC-based *in vitro* myelin formation assay by combining stem cell and microfluidic technologies that can be quantified by an automated method and is suitable for long-term live imaging. We believe that our assay constitutes a powerful tool to better understand myelination and to identify novel therapeutic avenues for treating dysmyelinating and demyelinating diseases such as MS and leukodystrophies. In its current form, our assay has already led us to investigate myelin wrapping and it has the potential to be modified, depending on the specific question being asked, and to be expanded and optimized to accommodate larger drug screening formats.

MATERIALS AND METHODS

Oligodendrocyte generation

A timeline representation of the process is provided in Fig. 1. Mouse D3 ESCs were grown on mouse embryonic fibroblast (MEF) plates by feeding with mouse ESC medium supplemented with 1000 U/ml mouse leukemia inhibitory factor (LIF; Millipore) every day. NPCs were generated and differentiated as modified from a previous study (Marchetto et al., 2008). On D1, OPC differentiation started by switching NPCs into differentiation medium, which comprised N2/B27 medium supplemented with IGF1 and PDGFα (R&D Systems). On D8, OPCs were switched to maturation medium, which comprised N2/B27 medium supplemented with CNTF, NT3 (NTF3) and T3 (Sigma-Aldrich). From D1, cells were fed every other day. For further details of culture media and conditions, see the supplementary Materials and Methods.

Myelinating co-cultures

Neurons were differentiated following a previously published protocol that enriches for cortical neurons (Gaspard et al., 2009). On D12, neurons were plated either on laminin-coated coverslips or in the neuronal compartment of microfluidic devices. Neurons were maintained in neuron medium for another 1-2 weeks for optimal neurite growth. Either 200,000 (coverslip) or 80,000 (device) oligodendrocytes at D15 of the differentiation protocol were plated on neurons. Every other day, co-cultures were fed with myelination medium, which comprises neuron medium supplemented with 40 ng/ml T3 (Sigma-Aldrich).

Microfluidic devices

Microfluidic devices were fabricated as described (Taylor et al., 2005). A detailed description of the fabrication is provided in the supplementary Materials and Methods.

Immunostaining

Cells were fixed in 4% paraformaldehyde in PBS for 15 min, blocked and permeabilized with horse serum (10%) and Triton X-100 (0.1%) in PBS and were incubated overnight with a combination of primary antibodies (see supplementary Materials and Methods). Images were acquired on Zeiss LSM confocal microscopes at 1, 0.5, 0.33 or 0.3 µm intervals and were processed with Zen (Zeiss), Imaris (Bitplane) and ImageJ (NIH).

Assessment of differentiation efficiency

On D8 and D15, cells were fixed and stained as described above. Images of six to ten randomly selected regions per well were taken on Stereo Investigator (MicroBrightField). Cell counts were performed using Cell Counter on ImageJ. The total number of cells was determined by DAPI staining. Three wells per experiment in two independent experiments were counted.

The expression levels on D8 and D15 were compared with undifferentiated NPCs (D0) by qPCR. The average fold changes of three independent experiments are shown. Three internal replicates were performed and averaged for each experiment. *Gapdh* expression was used for normalization. The primer pairs used are listed in supplementary material Table S2.

Electron microscopy and array tomography

Oligodendrocytes expressing GFP and neurons expressing RFP were grown on gridded glass-bottom dishes and fixed as described above. Regions of interest (ROIs) were located and their locations recorded for future use (supplementary material Fig. S6). The samples were embedded in Spurr's resin (EMS, 14300) and ROIs were marked by hand and later by the UV beam of a Zeiss PALM MicroBeam laser capture microdissection microscope (supplementary material Fig. S6). Transverse 70-nm sections were then taken of the ROI and imaged on a Zeiss Libra 120 PLUS for TEM.

After confirming wrapping events by TEM, 100-nm thick serial sections were taken from the same block using a similar device to that reported elsewhere (Horstmann et al., 2012). Sections were counterstained on the chip (supplementary material Fig. S6) and were then imaged in a Zeiss Sigma VP field emission scanning electron microscope using a four-quadrant solid-state backscatter detector with the quadrants inverted to produce a TEM-like image. Of the 52 serial sections taken, two were omitted due to sectioning and collection artifacts (slices 12 and 32). The resulting dataset was aligned, segmented and 3D rendered on TrackEM2 (FIJI) and Amira (FEI,). For further details of EM and array tomography, see the supplementary Materials and Methods.

Quantification of myelin formation

Images of the entire myelination compartment of each device were acquired as 15% overlapping tiles on confocal microscopes at 1-µm intervals and were stitched in Zen. A detailed description of the computational and manual methods is provided in the supplementary Materials and Methods, Fig. S4 and Appendix S1. Eleven devices from four independent experiments were quantified for total, GFP and nonGFP myelination. Five devices were quantified without T3 supplementation. Five devices for each condition were quantified manually to evaluate CEM.

Live imaging

In total, we observed 21 complete wrapping and 15 partial wrapping events. SARAPE was observed in all 21 of the complete wrapping events and anchored oligodendrocyte processes were observed in all 15 partial wrapping events. Although in most of these events a single oligodendrocyte process anchored at one location and wrapped the axon, an oligodendrocyte may have sent out more than one process to wrap different axons (as in Fig. 5; supplementary material Movie 1); in two cases (one complete and one partial wrapping), two processes of the same oligodendrocyte were anchored on the axon and wrapped the same segment (as in supplementary material Fig. S4 and Movie 2). Further details are provided in the supplementary Materials and Methods.

Development (2015) 142, 2213-2225 doi:10.1242/dev.116517

Statistical analysis

Error bars in all figures indicate s.e. For qPCR, graphs are presented in log scale; the error bars are represented as described (Sriramulu et al., 1999). *P*-values for myelin quantification were calculated using the Mann-Whitney *U*-test.

Virus production

Lentiviral reporter plasmids were derived from pCSC-SP-PW (Marr et al., 2004). A mouse *Mbp* promoter was utilized for oligodendrocyte-specific expression of EGFP (Gow et al., 1992). A human synapsin I (*SYN1*) promoter was utilized for neuron-specific expression (Kügler et al., 2001) of either tdTomato (Fig. 6; supplementary material Movie 1) or mCherry (supplementary material Fig. S5, Movie 2). EGFP and tdTomato were targeted to the cell membrane through the N-terminal acylation peptide of lymphocyte protein tyrosine kinase (LCK) (Zlatkine et al., 1997) with a five amino acid linker (GPVAT) separating the two protein regions. Lentiviruses were produced as described previously (Tiscornia et al., 2006). See also the supplementary Materials and Methods and Table S3 for oligonucleotides used for reporter plasmid generation.

Acknowledgements

We thank Ayad Ali and Ozlem H. Caglayan for technical assistance; Yury Sigal, Michael Adams and Jamie Kasuboski for microscopy assistance; Jane Peppard for helpful discussions concerning assay development; and Mary Lynn Gage for editorial comments. CEM is dedicated to the loving memories of Cem and Dilay Kerman, who were taken from us far too early.

Competing interests

The authors declare no competing or financial interests.

Author contributions

B.E.K. is the lead author and contributed to the concept, designed and performed experiments and analyzed the data. H.J.K. designed and manufactured the microfluidic devices and contributed to the design of experiments on these platforms. K.P. contributed to development of the myelin quantification method and overall data analysis. A.M. provided tissue culture and immunohistochemistry assistance and contributed to the development of differentiation and myelination protocols. S.G. provided immunohistochemistry and data analysis assistance. M.S.J. and J.A.J.F. performed EM analysis and advised on microscopy use. R.J. generated lentiviral constructs. K.J.C. and P.A. contributed to the concept and development of differentiation and myelination assay and edited the manuscript. F.H.G. is the senior author and contributed to the concept, analyzed the data, revised the manuscript and provided financial support. B.E.K., H.J.K., K.P. and F.H.G. wrote the manuscript. All authors read and approved the final manuscript.

Funding

The work was supported by funds from the National Multiple Sclerosis Society, the Sanofi and Salk Institute Discovery Award, the Christopher & Dana Reeve Foundation, the Leona M. and Harry B. Helmsley Charitable Trust and Annette Merle-Smith. Additional support was provided in part by a Crick-Jacobs Junior Fellowship (to K.P.), the National Institutes of Mental Health [MH101634, to K.P.] and a training grant from the California Institute for Regenerative Medicine (CIRM) (to H.J.K.). M.S.J. and J.A.J.F gratefully acknowledge financial support from the Waitt Advanced Biophotonics Center, W. M. Keck Foundation, National Cancer Institute (NCI) P30 Cancer Center Support Grant [CA014195-40] and the National Institute of Neurological Disorders and Stroke (NINDS) P30 Neuroscience Center Core Grant [NS072031-03A1]. Deposited in PMC for release after 12 months.

Supplementary material

Supplementary material available online at
http://dev.biologists.org/lookup/suppl/doi:10.1242/dev.116517/-/DC1

References

Asou, H., Hamada, K. and Sakota, T. (1995). Visualization of a single myelination process of an oligodendrocyte in culture by video microscopy. *Cell Struct. Funct.* **20**, 59-70.

Barres, B. A., Lazar, M. A. and Raff, M. C. (1994). A novel role for thyroid hormone, glucocorticoids and retinoic acid in timing oligodendrocyte development. *Development* **120**, 1097-1108.

Bauer, N. G., Richter-Landsberg, C. and Ffrench-Constant, C. (2009). Role of the oligodendroglial cytoskeleton in differentiation and myelination. *Glia* **57**, 1691-1705.

Baumann, N. and Pham-Dinh, D. (2001). Biology of oligodendrocyte and myelin in the mammalian central nervous system. *Physiol. Rev.* **81**, 871-927.

Brüstle, O., Jones, K. N., Learish, R. D., Karram, K., Choudhary, K., Wiestler, O. D., Duncan, I. D. and McKay, R. D. (1999). Embryonic stem cell-derived glial precursors: a source of myelinating transplants. *Science* **285**, 754-756.

Bunge, R. P., Bunge, M. B. and Bates, M. (1989). Movements of the Schwann cell nucleus implicate progression of the inner (axon-related) Schwann cell process during myelination. *J. Cell Biol.* **109**, 273-284.

Chen, Z., Ma, Z., Wang, Y., Li, Y., Lü, H., Fu, S., Hang, Q. and Lu, P.-H. (2010). Oligodendrocyte–spinal cord explant co-culture: an in vitro model for the study of myelination. *Brain Res.* **1309**, 9-18.

Cummings, B. J., Uchida, N., Tamaki, S. J., Salazar, D. L., Hooshmand, M., Summers, R., Gage, F. H. and Anderson, A. J. (2005). Human neural stem cells differentiate and promote locomotor recovery in spinal cord-injured mice. *Proc. Natl. Acad. Sci. USA* **102**, 14069-14074.

Dean, J. M., Riddle, A., Maire, J., Hansen, K. D., Preston, M., Barnes, A. P., Sherman, L. S. and Back, S. A. (2011). An organotypic slice culture model of chronic white matter injury with maturation arrest of oligodendrocyte progenitors. *Mol. Neurodegener.* **6**, 46.

Douvaras, P., Wang, J., Zimmer, M., Hanchuk, S., O'Bara, M. A., Sadiq, S., Sim, F. J., Goldman, J. and Fossati, V. (2014). Efficient generation of myelinating oligodendrocytes from primary progressive multiple sclerosis patients by induced pluripotent stem cells. *Stem Cell Rep.* **3**, 250-259.

Eisenbach, M., Kartvelishvily, E., Eshed-Eisenbach, Y., Watkins, T., Sorensen, A., Thomson, C., Ranscht, B., Barnett, S. C., Brophy, P. and Peles, E. (2009). Differential clustering of Caspr by oligodendrocytes and Schwann cells. *J. Neurosci. Res.* **87**, 3492-3501.

Gaspard, N., Bouschet, T., Herpoel, A., Naeije, G., van den Ameele, J. and Vanderhaeghen, P. (2009). Generation of cortical neurons from mouse embryonic stem cells. *Nat. Protoc.* **4**, 1454-1463.

Gow, A., Friedrich, V. L., Jr and Lazzarini, R. A. (1992). Myelin basic protein gene contains separate enhancers for oligodendrocyte and Schwann cell expression. *J. Cell Biol.* **119**, 605-616.

Gupta, N., Henry, R. G., Strober, J., Kang, S.-M., Lim, D. A., Bucci, M., Caverzasi, E., Gaetano, L., Mandelli, M. L., Ryan, T. et al. (2012). Neural stem cell engraftment and myelination in the human brain. *Sci. Transl. Med.* **4**, 155ra137.

Hayworth, K. J., Kasthuri, N., Schalek, R. and Lichtman, J. W. (2006). Automating the collection of ultrathin serial sections for large volume TEM reconstructions. *Microsc. Microanal.* **12**, 86-87.

Horstmann, H., Körber, C., Sätzler, K., Aydin, D. and Kuner, T. (2012). Serial section scanning electron microscopy (S3EM) on silicon wafers for ultra-structural volume imaging of cells and tissues. *PLoS ONE* **7**, e35172.

Ioannidou, K., Anderson, K. I., Strachan, D., Edgar, J. M. and Barnett, S. C. (2012). Time-lapse imaging of the dynamics of CNS glial-axonal interactions in vitro and ex vivo. *PLoS ONE* **7**, e30775.

Jessen, K. R. and Mirsky, R. (2005). The origin and development of glial cells in peripheral nerves. *Nat. Rev. Neurosci.* **6**, 671-682.

Jiang, P., Selvaraj, V. and Deng, W. (2010). Differentiation of embryonic stem cells into oligodendrocyte precursors. *J. Vis. Exp.*, e1960.

Knobler, R. L., Stempak, J. G. and Laurencin, M. (1976). Nonuniformity of the oligodendroglial ensheathment of axons during myelination in the developing rat central nervous system. A serial section electron microscopical study. *J. Ultrastruct. Res.* **55**, 417-432.

Kügler, S., Meyn, L., Holzmüller, H., Gerhardt, E., Isenmann, S., Schulz, J. B. and Bähr, M. (2001). Neuron-specific expression of therapeutic proteins: evaluation of different cellular promoters in recombinant adenoviral vectors. *Mol. Cell. Neurosci.* **17**, 78-96.

Lee, S., Leach, M. K., Redmond, S. A., Chong, S. Y. C., Mellon, S. H., Tuck, S. J., Feng, Z.-Q., Corey, J. M. and Chan, J. R. (2012). A culture system to study oligodendrocyte myelination processes using engineered nanofibers. *Nat. Methods* **9**, 917-922.

Liu, S., Qu, Y., Stewart, T. J., Howard, M. J., Chakrabortty, S., Holekamp, T. F. and McDonald, J. W. (2000). Embryonic stem cells differentiate into oligodendrocytes and myelinate in culture and after spinal cord transplantation. *Proc. Natl. Acad. Sci. USA* **97**, 6126-6131.

Marchetto, M. C. N., Muotri, A. R., Mu, Y., Smith, A. M., Cezar, G. G. and Gage, F. H. (2008). Non-cell-autonomous effect of human SOD1 G37R astrocytes on motor neurons derived from human embryonic stem cells. *Cell Stem Cell* **3**, 649-657.

Marr, R. A., Guan, H., Rockenstein, E., Kindy, M., Gage, F. H., Verma, I., Masliah, E. and Hersh, L. B. (2004). Neprilysin regulates amyloid Beta peptide levels. *J. Mol. Neurosci.* **22**, 5-12.

Miron, V. E., Kuhlmann, T. and Antel, J. P. (2011). Cells of the oligodendroglial lineage, myelination, and remyelination. *Biochim. Biophys. Acta* **1812**, 184-193.

Nave, K.-A. (2010). Myelination and support of axonal integrity by glia. *Nature* **468**, 244-252.

Numasawa-Kuroiwa, Y., Okada, Y., Shibata, S., Kishi, N., Akamatsu, W., Shoji, M., Nakanishi, A., Oyama, M., Osaka, H., Inoue, K. et al. (2014). Involvement of ER stress in dysmyelination of pelizaeus-merzbacher disease with PLP1 missense mutations shown by iPSC-derived oligodendrocytes. *Stem Cell Rep.* **2**, 648-661.

Padmanabhan, K., Eddy, W. F. and Crowley, J. C. (2010). A novel algorithm for optimal image thresholding of biological data. *J. Neurosci. Methods* **193**, 380-384.
Pedraza, L., Huang, J. K. and Colman, D. (2009). Disposition of axonal caspr with respect to glial cell membranes: Implications for the process of myelination. *J. Neurosci. Res.* **87**, 3480-3491.
Peru, R. L., Mandrycky, N., Nait-Oumesmar, B. and Lu, Q. R. (2008). Paving the axonal highway: from stem cells to myelin repair. *Stem Cell Rev.* **4**, 304-318.
Potter, G. B., Rowitch, D. H. and Petryniak, M. A. (2011). Myelin restoration: progress and prospects for human cell replacement therapies. *Arch. Immunol. Ther. Exp.* **59**, 179-193.
Pouya, A., Satarian, L., Kiani, S., Javan, M. and Baharvand, H. (2011). Human induced pluripotent stem cells differentiation into oligodendrocyte progenitors and transplantation in a rat model of optic chiasm demyelination. *PLoS ONE* **6**, e27925.
Quarles, R. H. (2002). Myelin sheaths: glycoproteins involved in their formation, maintenance and degeneration. *Cell. Mol. Life Sci.* **59**, 1851-1871.
Remahl, S. and Hildebrand, C. (1990a). Relations between axons and oligodendroglial cells during initial myelination. II. The individual axon. *J. Neurocytol.* **19**, 883-898.
Remahl, S. and Hildebrand, C. (1990b). Relation between axons and oligodendroglial cells during initial myelination. I. The glial unit. *J. Neurocytol.* **19**, 313-328.
Siegel, G. J. (2006). *Basic Neurochemistry: Molecular, Cellular, and Medical Aspects*, pp. 51-71. Amsterdam: Elsevier.
Snaidero, N., Möbius, W., Czopka, T., Hekking, L. H. P., Mathisen, C., Verkleij, D., Goebbels, S., Edgar, J., Merkler, D., Lyons, D. A. et al. (2014). Myelin membrane wrapping of CNS axons by PI(3,4,5)P3-dependent polarized growth at the inner tongue. *Cell* **156**, 277-290.
Sobottka, B., Ziegler, U., Kaech, A., Becher, B. and Goebels, N. (2011). CNS live imaging reveals a new mechanism of myelination: the liquid croissant model. *Glia* **59**, 1841-1849.
Song, B., Sun, G., Herszfeld, D., Sylvain, A., Campanale, N. V., Hirst, C. E., Caine, S., Parkington, H. C., Tonta, M. A., Coleman, H. A. et al. (2012). Neural differentiation of patient specific iPS cells as a novel approach to study the pathophysiology of multiple sclerosis. *Stem Cell Res.* **8**, 259-273.
Sriramulu, S., Jarvi, T. D. and Stuve, E. M. (1999). Reaction mechanism and dynamics of methanol electrooxidation on platinum(111). *J. Electroanal. Chem.* **467**, 132-142.
Stancic, M., Slijepcevic, D., Nomden, A., Vos, M. J., de Jonge, J. C., Sikkema, A. H., Gabius, H.-J., Hoekstra, D. and Baron, W. (2012). Galectin-4, a novel neuronal regulator of myelination. *Glia* **60**, 919-935.
Taylor, A. M., Blurton-Jones, M., Rhee, S. W., Cribbs, D. H., Cotman, C. W. and Jeon, N. L. (2005). A microfluidic culture platform for CNS axonal injury, regeneration and transport. *Nat. Methods* **2**, 599-605.
Tiscornia, G., Singer, O. and Verma, I. M. (2006). Production and purification of lentiviral vectors. *Nat. Protoc.* **1**, 241-245.
Tsuji, O., Miura, K., Okada, Y., Fujiyoshi, K., Mukaino, M., Nagoshi, N., Kitamura, K., Kumagai, G., Nishino, M., Tomisato, S. et al. (2010). Therapeutic potential of appropriately evaluated safe-induced pluripotent stem cells for spinal cord injury. *Proc. Natl. Acad. Sci. USA* **107**, 12704-12709.
Watkins, T. A., Emery, B., Mulinyawe, S. and Barres, B. A. (2008). Distinct stages of myelination regulated by γ-secretase and astrocytes in a rapidly myelinating CNS coculture system. *Neuron* **60**, 555-569.
Yang, I. H., Gary, D., Malone, M., Dria, S., Houdayer, T., Belegu, V., McDonald, J. W. and Thakor, N. (2012). Axon myelination and electrical stimulation in a microfluidic, compartmentalized cell culture platform. *Neuromolecular Med.* **14**, 112-118.
Zhang, H., Jarjour, A. A., Boyd, A. and Williams, A. (2011). Central nervous system remyelination in culture—a tool for multiple sclerosis research. *Exp. Neurol.* **230**, 138-148.
Zlatkine, P., Mehul, B. and Magee, A. I. (1997). Retargeting of cytosolic proteins to the plasma membrane by the Lck protein tyrosine kinase dual acylation motif. *J. Cell Sci.* **110**, 673-679.

SUPPLEMENTARY MATERIALS AND METHODS

Automated myelin quantification

The following is a detailed description of how the images were processed and the myelin was identified. CEM was developed to automate these operations. Its outputs include the resulting images and calculated values for each parameter as well as myelination percentages.

Generation of binary image stacks: First, the confocal stacks were split into single channel stacks (MBP-, TUJ1-, GFP- and DAPI-stacks). The brightness of each stack was adjusted to maximize the signal-to-noise ratio. A reference slice, one with a large amount of positive signal and low background noise, was selected for each stack independently. The binary conversion was done using ImageJ's built-in "Make Binary" function using IsoData method and dark background. Instead of calculating thresholds for each slice, the values from reference slice were used for the entire stack. The resulting image has two pixel values, 0 for black and 255 for white.

Cell body removal: We used "AND" operator of the built-in "Image Calculator" (ImageJ) to identify nuclei of oligodendrocytes (Binary-DAPI-stack "AND" Binary-MBP-stack) and of neurons (Binary-DAPI-stack "AND" Binary-TUJ1-stack). The resulting images were cleaned of noise via the "Despeckle" function and the multiple nuclei were divided into single nuclei via the "Watershed" function. We called these stacks of images Oligodendrocyte-Nuclei and Neurons-Nuclei, respectively. The MATLAB CEM GUI was used to remove particles whose area was smaller than 50 pixels square (using the MATLAB function "exclude") to eliminate nuclei partially overlapping with cell bodies. The remaining nuclei were dilated for 5 pixels to grow the nuclei into cell bodies using the MATLAB "imdilate" function. The 5-pixel dilation was performed by using a disk of radius 5 across the image. The resulting images were called Oligodendrocyte-Cell-Bodies and Neurons(plural?)-Cell-Bodies. Next, using ImageJ, cell bodies images were "Inverted" (ImageJ function), i.e., all 0 pixel values were turned into 255 and vice versa. When this image was "Multiplied" (an operator in ImageJ's "Image Calculator") to the corresponding binary image, i.e., Oligodendrocyte-Cell-Bodies "Multiplied" to Binary-MBP-stack, the result was the cell bodies removed (CBR-MBP-stack) image.

Identification of subsets of axons: Similar to nuclei identification "ANDing" binary TUJ1-stack (CBR or not) with the binary GFP-stack resulted in GFP-positive neurons (Marker-positive-axons). Next, we "Inverted" the Marker-positive-axon image and "Multiplied" it back to a binary TUJ1 image to identify nonGFP neurons (Marker-negative-axons).

Identification of myelin: We defined myelin as the overlap between the binary oligodendrocyte image and binary axon or subset of axon images. The overlap was identified via the "AND" operator. The total myelin for the entire device was identified by "ANDing" binary CBR-MBP-stack with the binary CBR-TUJ1-stack and resulting in CBR-Overlap-All image. The myelin for GFP and nonGFP axons was identified by "ANDing" binary CBR-MBP-stack to Marker-positive-axons and Marker-negative-axons, respectively.

Calculation of results: The results were generated as pixel counts and percent values. The pixels were counted using the "Histogram" function of ImageJ on maximum intensity projections. For example, applying "Histogram" function on CBR-TUJ1-stacks gave the number of TUJ1-positive pixels after cell body removal, which was defined as all axons here. While applying the "Histogram" function on maximum intensity, projected CBR-Overlap-All gave the total pixel count of myelin. The percent of myelinated axons was calculated by dividing the latter by the former and multiplying by 100. Similar calculations were performed for other values.

Manual myelin quantification

The length of each myelin segment was measured using the "Segmented Line" tool on ImageJ (NIH) for the entire myelination compartment. The lengths in pixels were summed for each sample, giving the total myelin of that sample. Total myelin for each condition was averaged and the average value for +T3 was used for normalization, as described in the manuscript.

Overlap Probability Calculations

We first determined the probability of a pixel being MBP positive P(MBP) and the probability of a pixel being TUJ1 positive P(Axon) within the myelination compartment independently for each experiment. The joint probability of a pixel being positive for both due entirely to chance was calculated as P(MBP)*P(Axon). We compared this chance probability for the +T3 condition to the myelin ratio observed for +T3 experimentally P(MBP | Axon) and these were significantly different ($p=0.0025$, N=11, Wilcoxon Ranksum). Similarly, the chance overlap in the -T3 condition as compared to the overlap observed from the -T3 experimental data was significantly different ($p=0.0079$, N=5, Ranksum), suggesting the myelination effects observed were not due to chance. Additionally, this method allowed us to examine how much the myelin overlap calculation was sensitive to changes in the MBP amount. To explore this question, we first determined the percent difference in MBP positive pixels in the +T3 and -T3 conditions (mean difference = 15%). Following this, the total number of MBP positive pixels was reduced by this amount so that the population's MBP means were now equal for +T3 and -T3. From this, we compared the myelin overlap for the "equalized T3" and the original -T3. Again, we found that these groups were significantly different ($p=0.0192$, N=11 T3, N=5 non-T3, Wilcoxon Ranksum), suggesting that the changes in myelination observed could not be accounted for due to changes in the MBP alone.

Cell culture methods and media compositions

Mouse ESC Medium consisted of, KnockOut DMEM (Life Technologies), 15% KnockOut serum replacement (Life Technologies), GlutaMAX (Life Technologies), 1x non-essential amino acids (Gibco), and 55 µM 2-mercaptoethanol (Gibco).

NPCs were generated and differentiated as described below that was modified from a previous study (Marchetto et al., 2008). ESCs were grown in suspension in mouse ESC

Medium without LIF for the first day and in N2/B27 Medium supplemented with 500 ng/ml Noggin (PeproTech) for four more days. Next, embryoid bodies were dissociated, plated on and maintained on laminin- (Life Technologies) coated dishes in N2/B27 Medium supplemented with 20 ng/ml Epidermal growth factor (EGF;PeproTech), 20 ng/ml Fibroblast growth factor-basic (bFGF; Stemgent).

N2/B27 Medium: DMEM/F12-Glutamax Medium (Gibco), 1x N2 supplement (Gibco), 1x B27 supplement (Gibco).

Differentiation Medium: N2/B27 Medium supplemented with 10 ng/ml Insulin-like growth factor 1 (IGF-1; R&D Systems), 10 ng/ml Platelet-derived grow factor-α (PDGF-α; R&D Systems).

Maturation Medium: N2/B27 Medium supplemented with 10 ng/ml Ciliary neurotrophic factor (CNTF; Sigma-Aldrich), 5 ng/ml Neurotrophin-3 (NT3; Sigma-Aldrich) + 40 ng/ml Triiodothyronine (T3; Sigma-Aldrich).

Neuron Medium, which was described before (Gaspard et al., 2009), consisted of, 1:1 DDM Medium:Neurobasal/B27 Medium supplemented with 20 ng/ml Glial cell derived neurotrophic factor (GDNF; R&D Systems), 500 µg/ml cAMP (Sigma), and 0.2 µM ascorbic acid (Sigma).

Microfluidic devices

Microfluidic devices were fabricated as described previously (Taylor et al., 2005). Two layers of SU-8 photoresist, 3 µm high microgrooves and 100 µm high channels, were generated on a silicon wafer by using standard photolithography techniques. To fabricate microfluidic devices, 1:10 ratio of curing agent and poly-dimethly-siloxane (PDMS, Sylgard 184, Dow Corning Co.) was mixed and cured on that master mold. The enclosed channel on one side was cut out to achieve the open well design (Fig. 4A; supplementary material Fig. S3B). The microgrooves were 10 µm wide, 3 µm high and 150 µm long. Glass coverslips (Fisher Scientific) were coated with 0.5 mg/mL poly-L-lysine (Sigma); then the devices were assembled onto coverslips, followed by coating with laminin (Life Technologies) in basal medium.

Immunostaining

Primary antibodies used were: 1:1,000 mouse or rabbit anti-TUJ1 (Covance, MMS-435P and PRB-435P), 1:50 rat anti-MBP (Serotec, MCA409S), 1:400 mouse anti-Caspr (UC Davis/NIH NeuroMab Facility, 75-001), 1:400 rabbit anti-PDGFRα (Santa Cruz Biotechnology, sc-338), 1:200 rabbit anti-NG2 (Millipore, AB5320), 1:500 mouse anti-Olig1 (Millipore, MAB5540), 1:500 rabbit anti-Olig2 (Millipore, AB9610), 1:200 rabbit anti-Sox10 (Millipore, AB5727), 1:1000 chicken anti-GFAP (Millipore, AB5541), 1:1000 chicken anti-P0 (Aves Labs, PZO) and 1:500 goat anti-PMP22 (Santa Cruz Biotechnology, sc-18535). For O4 staining, 1:40 mouse anti-O4 (R&D Systems, MAB1326) was added to the medium for 30 min prior to fixation and permeabilization. DAPI (Sigma) was used to visualize nuclei.

Electron microscopy

Oligodendrocytes expressing GFP and neurons expressing RFP were grown on gridded glass-bottomed dishes and fixed as described above. Regions of interest were located and their locations were recorded for future use (supplementary material Fig. S6A).

Next, samples were secondarily fixed overnight in 2.5% glutaraldehyde in PBS. The samples were then fixed in 1% osmium tetroxide/0.3% potassium ferrocyanide in buffer for one hour on ice, washed in water, and *en bloc* stained with 2% aqueous uranyl acetate for one hour on ice. After staining, the samples were dehydrated in a graded ethanol series and embedded in Spurr's resin.

Once the resin was cured, the glass coverslips were removed with hydrofluoric acid and regions of interest were marked by hand and later by the UV beam of a laser capture microdissection microscope (supplementary material Fig. S6A; Zeiss PALM MicroBeam, Jena, Germany). 70-nm cross sections were then taken of the region of interest and imaged on a TEM at 120 KeV (Zeiss Libra 120 PLUS, Oberkochen, Germany)

Dense Wrapping Measurements:

Thick sections were taken and imaged on the TEM as described above for regions that demonstrated dense wrapping. The resulting images were rotated from -90 degrees to +90 degrees in 1 degree steps using a nearest neighbor approximation. A ROI was created at 30 pixels in height (Y-dimension), and a line profile was generated by averaging the pixel intensity values along the y-dimension of the ROI. The raw data from the line profile was smoothed using a low-pass filter with filter coefficients equal to the reciprocal of the span (ie. Moving average).Following this, the lowest four peaks were found using peak analysis.

Array Tomography

After confirming wrapping events by TEM, 100nm thick serial sections were taken from the same block using a similar device as reported elsewhere (Horstmann et al., 2012), chloroform spread, and placed onto silica wafer chips (Ted Pella, Cat. #16007). The sections were counterstained on the chip with 2% uranyl acetate for 10 minutes followed by 0.4% lead citrate for 4 minutes. Post staining, the chip was subsequently mounted and grounded to an aluminum stub with silver paint. The sections were then imaged in a FE-SEM (Zeiss Sigma VP, Cambridge, UK) at 15 KeV with a 30µm aperture using a 4-quadrant solid-state backscatter detector with the quadrants inverted to produce a TEM-like image. Images were acquired at 12,012 x 6,876 pixels at 2 nm/pixel with a dwell time of 3.5 µs and a line average of 4 using the ATLAS scan engine (Fibics Inc., Ottawa, Canada). Of the 52 serial sections taken, two were omitted due to sectioning and collection artifacts (Slices 12 and 32). The resulting dataset was then stacked and aligned using an affine transform in TrackEM2 (FIJI) and exported to Amira (FEI, Netherlands) for segmentation and 3D rendering. The resulting model was smoothed for appearance purposes by reducing surface details using Amira's built-in smoothing algorithms.

Live imaging

For live imaging, co-cultures were grown either on glass-bottom dishes (GWSt-3522; WillCo Wells) or in microfluidic devices assembled on coverslips. The latter were later attached to a 35-mm plastic dish with a hole in the middle prior to imaging. Neurons were infected with a lentiviral construct expressing either mCherry or membrane-localized TdTomato three to four days prior to initiation of co-culture. Oligodendrocytes were infected with a lentiviral construct expressing membrane-localized EGFP three to four days prior to initiation of co-culture. Imaging was performed on a Zeiss CSU Spinning Disk Confocal Microscope equipped with a stage-top incubation system or on a Yokogawa Cell Voyager 1000 Spinning Disk Confocal Microscope. Optical z-sections were 1 μm apart. Images were taken every 10 min.

Production of viral constructs

The viral vectors were constructed starting from the plasmid pCSC-Syn-EGFP, which was first modified by insertion of a multiple cloning site, provided by double strand DNA cassette (oligonucleotides G17 and G18), to produce pCSC-Syn-mcs-EGFP. The latter was used to isolate the vectors pCSC-Syn-mcs-mCherry and pCSC-Syn-mcs-tdTomato by replacing the EGFP coding sequence with the PCR amplified mCherry sequence (primers G21 and G22) and tdTomato sequence (primers G23 and G22). pCSC-Syn-mcs-EGFP was also used to derive vector pCSC-MBP-mcs-EGFP, wherein the MBP promoter, obtained by PCR amplification (primers G52 and G53) from the plasmid pMG2-1 (courtesy of A. Gow; Gow et al., 1992), was introduced in place of the Syn promoter. Finally, pCSC-MBP-LckN-EGFP was derived from pCSC-MBP-mcs-EGFP by introducing a double strand DNA cassette (oligonucleotides G54 and G55) encoding the Lck membrane localization domain in the multiple cloning site. pCSC-Syn-LckN-tdTomato was obtained from pCSC-Syn-mcs-tdTomato in a similar way. All constructs include a canonical Kozak sequence and were verified by DNA sequencing. The oligonucleotides used are given in supplementary material Table S3.

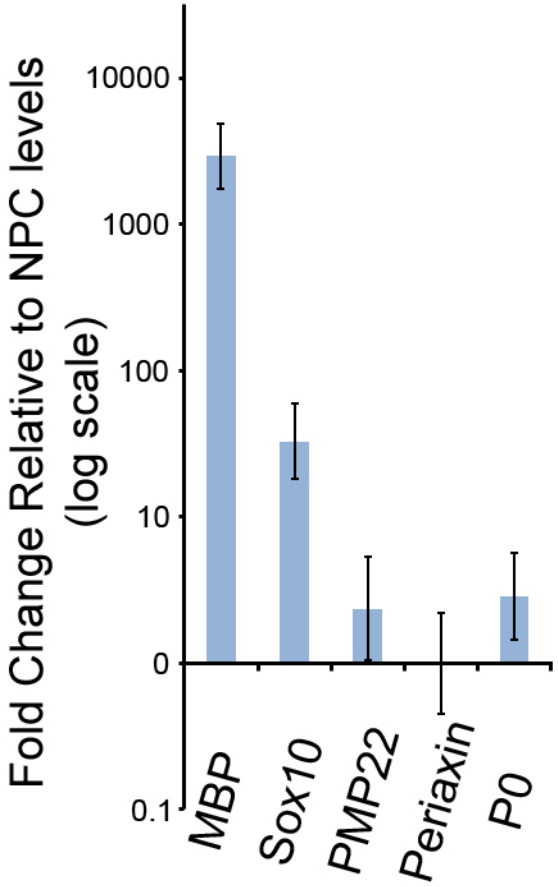

Supplementary Figure S1: Expression level analysis of Schwann cell-specific genes by quantitative-PCR. MBP and Sox10 expression levels are also shown as a reference. Fold changes in expression levels compared to undifferentiated NPCs were plotted in Log-scale. GAPDH expression was used for normalization.

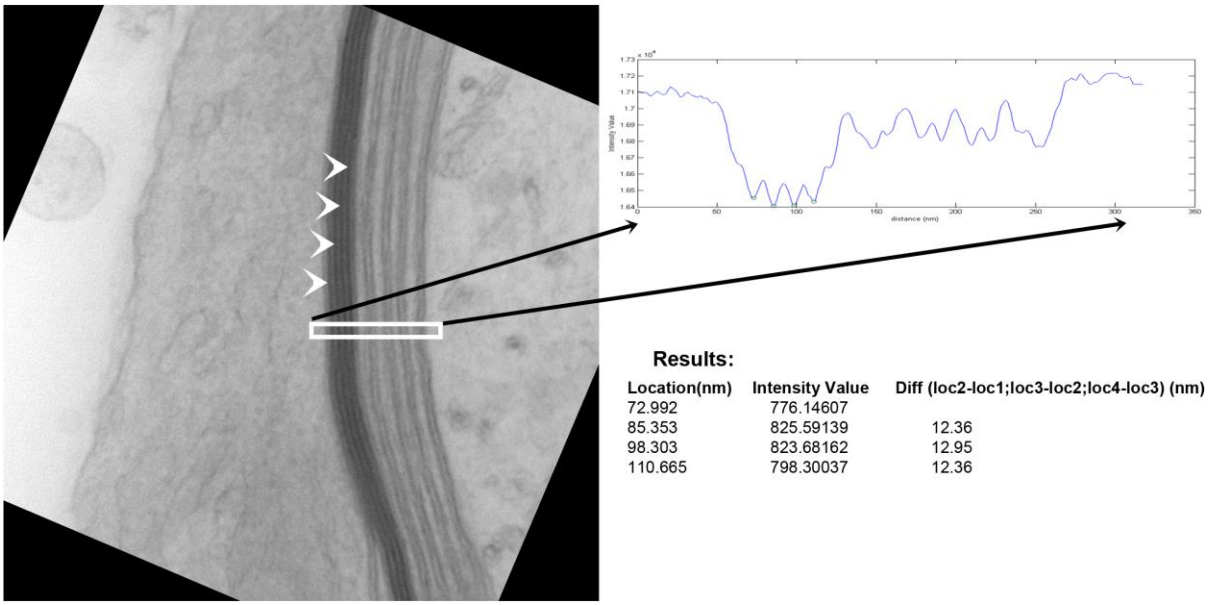

Supplementary Figure S2: Measurement of distance between major dense lines. The intensity of the pixels across compact myelin of an high magnification EM image was measured. The distances between four major dense lines (arrowheads) were shown in nm.

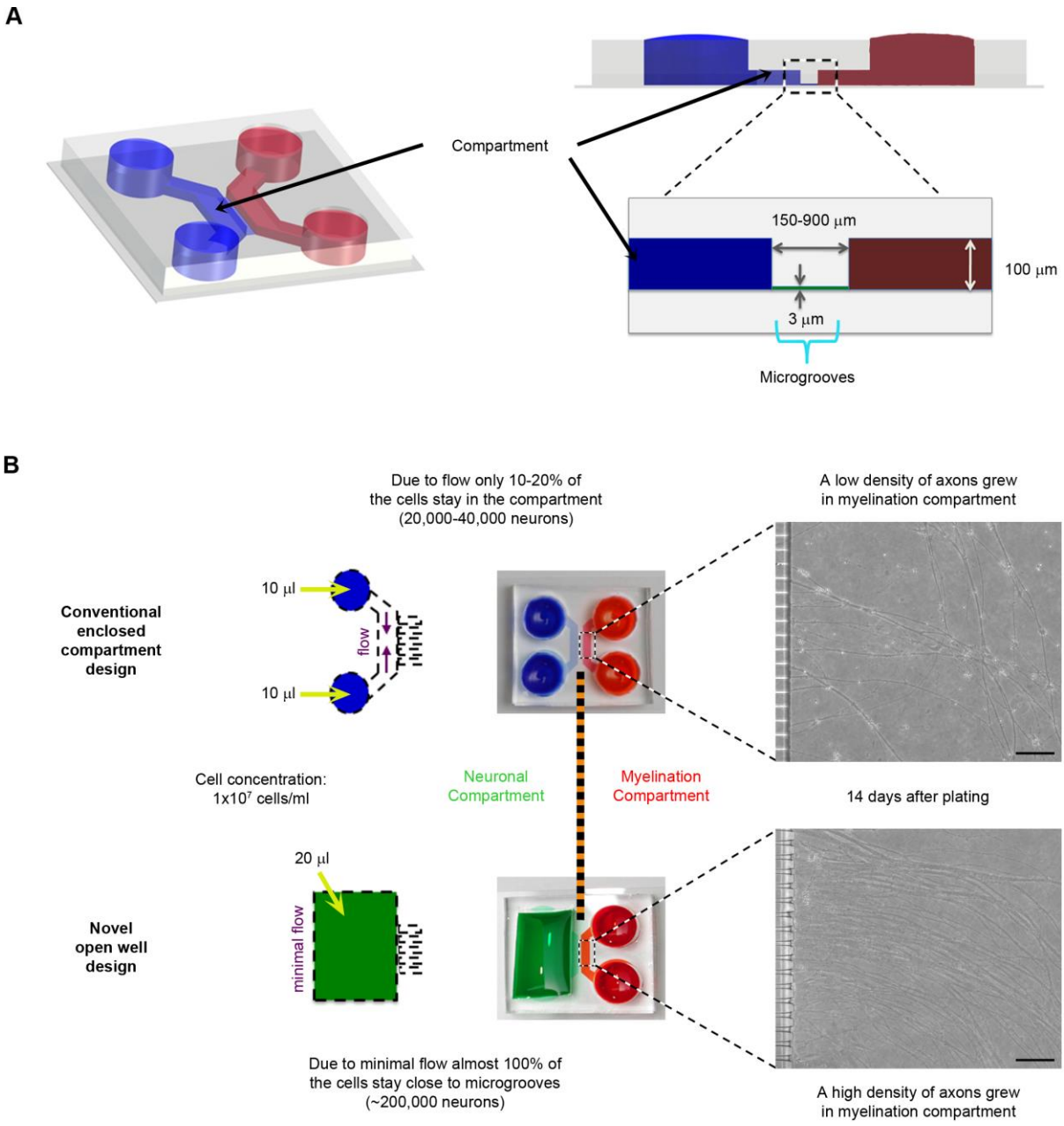

Supplementary Figure S3: Microfluidic devices. (**A**) A 3D model (right) and schematic cross-sections (left) of conventional microfluidic devices. Two enclosed main compartments (blue and red; 100 µm high) are interconnected via microgrooves (3 µm high, 10 µm wide, and 150-900 µm long). (**B**) A comparison of enclosed compartment (upper half) and open well (lower half) microfluidic devices. Left portion shows schematic representations of flow affecting the number of neurons that stay close to microgrooves. Images of actual devices are in the middle. Representative images of axons growing into myelination compartment in two designs are on the right. Scale bars: 150 µm.

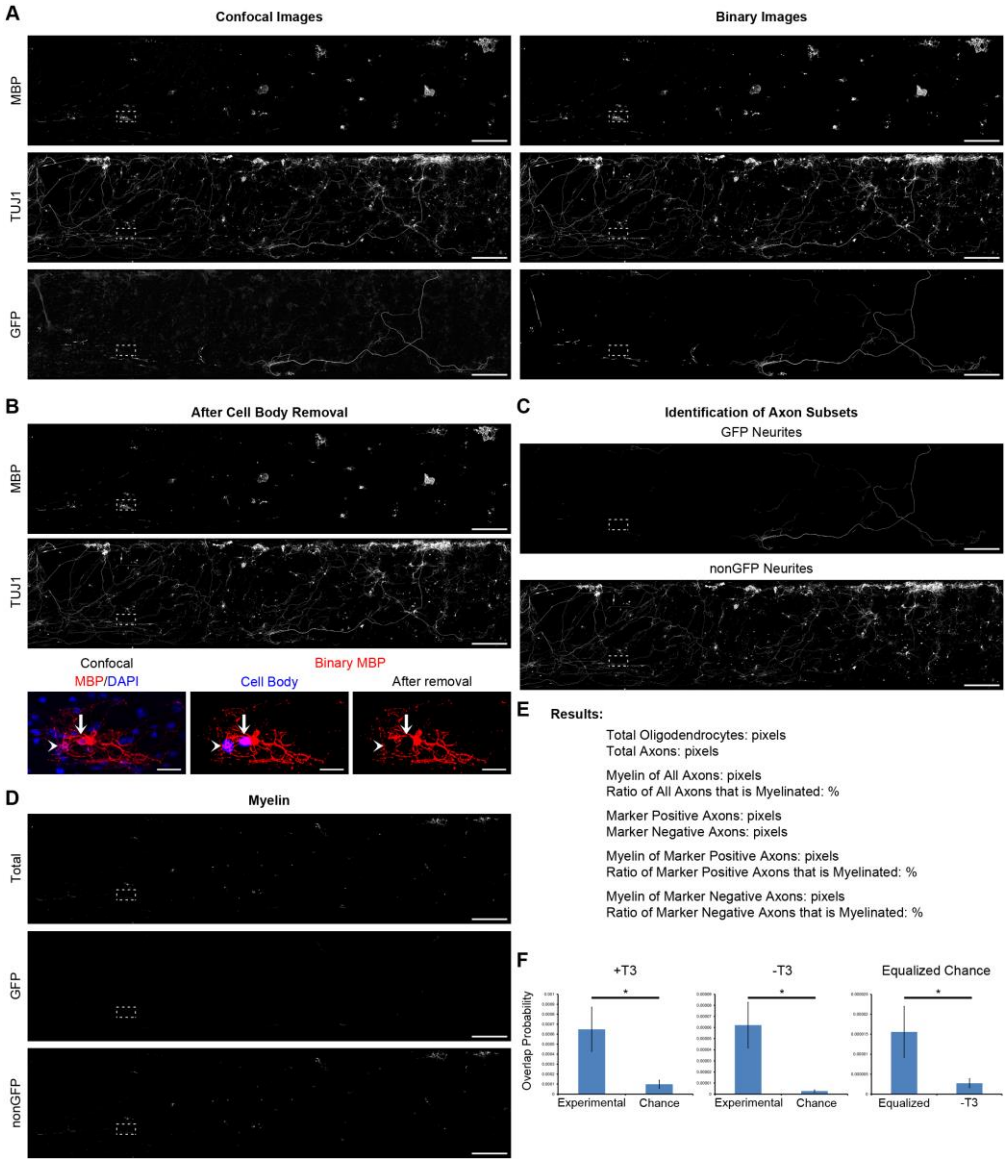

Supplementary Figure S4: Quantification of myelin formation. (**A**) Confocal and binary single channel images of merged images in Fig 5A,B. (**B**) Oligodendrocytes (MBP) and neurons (TUJ1) after processing to remove cell bodies. Upper panels: the entire myelination compartment; lower panels: a close-up of the boxed regions in Fig. 5 and S2. Nuclei (blue) identified and grown into cell bodies (blue; arrow). Some nuclei overlap with a large portion of MBP-positive membrane, resulting in false cell body identification (blue; arrowhead). Gaps were left in MBP binary channel after removal (arrow and arrowhead). (**C**) Identified GFP-positive and -negative subsets of axons. (**D**) Identified overlap for the entire myelination compartment of all neurites (Total), of neurites of GFP-expressing neurons (GFP) and of neurites of neurons not expressing GFP (nonGFP). (**E**) CEM output values shown in the panel as pixel counts and percent values. See also the accompanying Users' Guide for CEM. (**F**) Conformation of myelin quantification through comparison between probabilities of experimentally calculated overlap and pure chance overlap (left panels) and equalized probabilities (right panel). See supplementary materials and methods for calculation details. Scale bars: 500 µm.

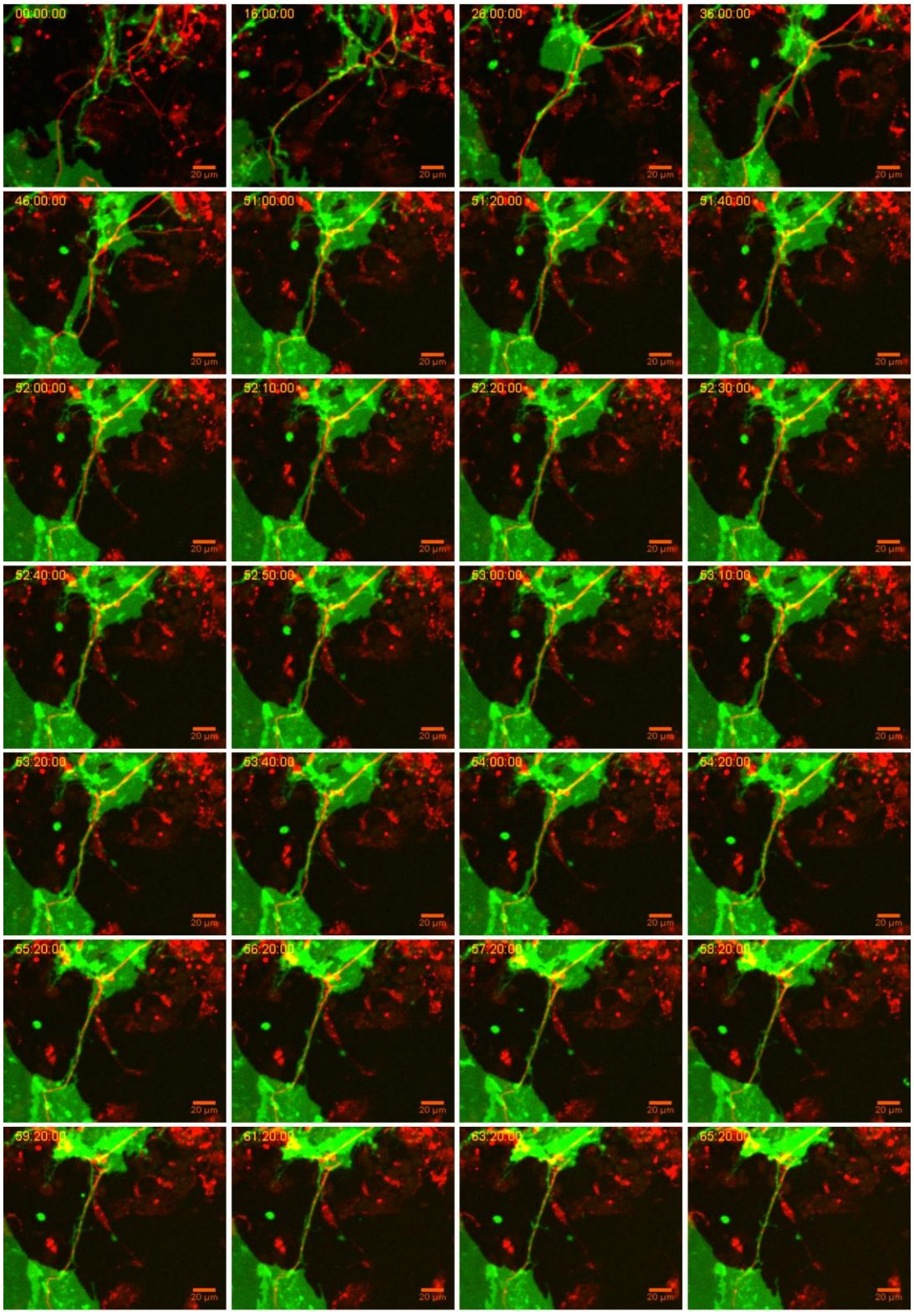

Supplementary Figure S5: Selected frames from Supplementary Movie 2. The time-frame focuses on a single wrapping event. Note that the oligodendrocyte sending out the two processes that wrap the axon is out of the viewing frame. Scale bars: 20 µm.

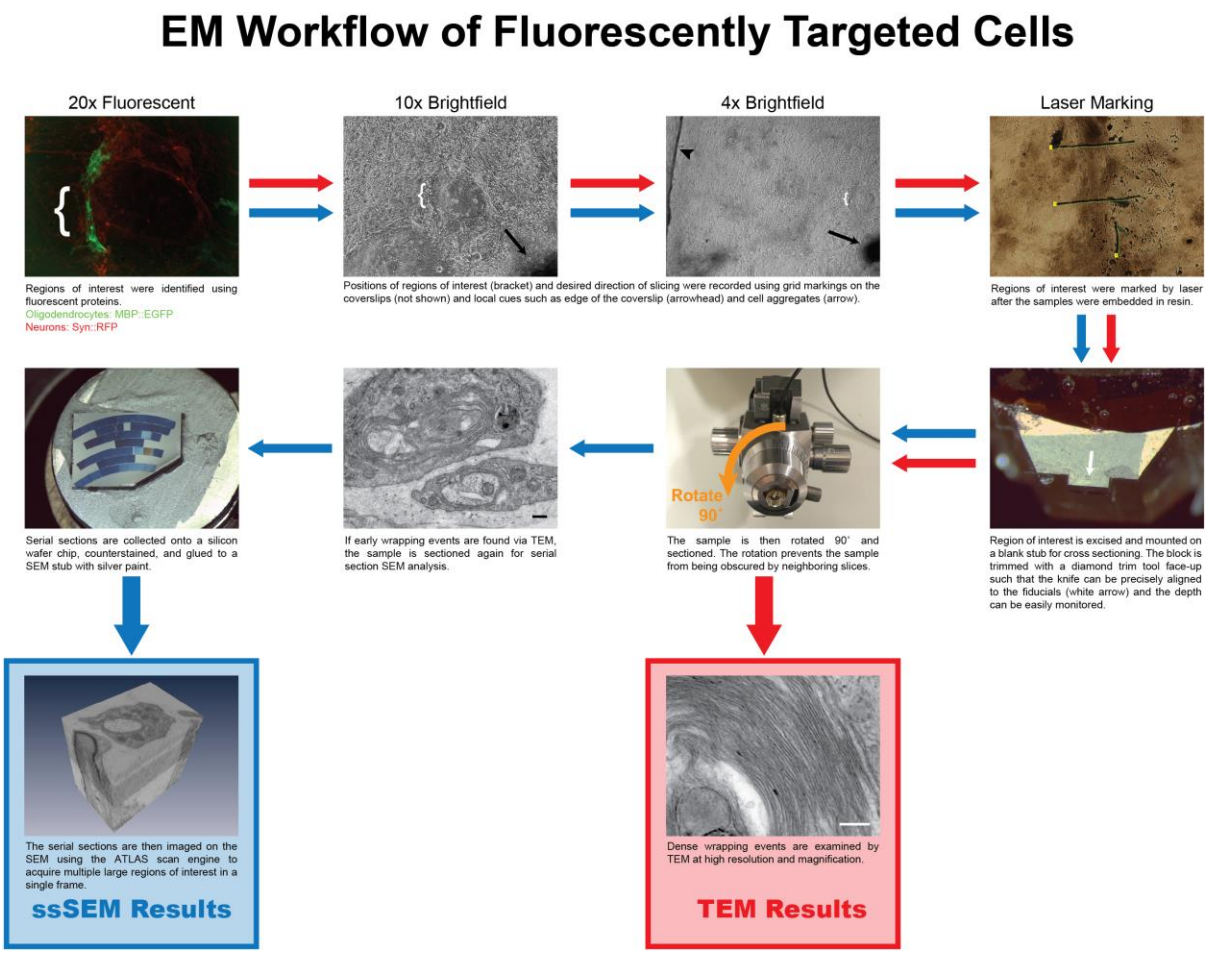

Supplementary Figure S6: Electron microscopy workflow of fluorescently tagged cells. The workflow describes how EM data was collected from fluorescently tagged cells. Briefly, regions of interest (ROI) were located via fluorescence and features were noted in brightfield mode at lower magnifications. After EM processing, ROIs were found again using the features noted in brightfield and cutting windows were made using a UV laser. The sample was then trimmed and sectioned either for high-resolution TEM of dense wrapping regions or for serial section SEM (ssSEM) of early wrapping regions. Note: the laser marking and EM images are not from the same dataset but rather were used for demonstration purposes of the procedure. Scale bars: 250nm.

Supplementary Table S1. Percentages and total number of cells counted for assessing differentiation efficiency.

Day 8				
Marker	**Percent total cells**	**Standard error**	**Number of cells expressing the marker**	**Total number of cells**
NG2	37.83	2.44	3201	8,486
PDGF-Rα	37.07	3.54	4007	10,385
Olig1	66.41	1.14	6904	10,385
Olig2	66.56	2.72	6942	10,548
Sox10	85.61	1.37	6431	7,568
O4	2.21	0.24	158	8,469
MBP	0.12	0.04	203	10,385
GFAP	5.09	0.83	402	8,486
TUJ1	9.69	2.13	790	7,568
Day 15				
Marker	**Percent total cells**	**Standard error**	**Number of cells expressing the marker**	**Total number of cells**
NG2	29.19	2.28	1941	6,457
PDGF-Rα	15.69	2.67	885	5,804
Olig1	41.90	4.49	2362	5,804
Olig2	53.48	4.76	4448	8,583
Sox10	63.54	4.78	4981	7,850
O4	13.10	0.79	674	11,236
MBP	4.59	1.31	250	5,804
GFAP	5.08	1.23	337	6,457
TUJ1	8.38	1.69	699	7,850

Supplementary Table S2. Primers used for quantitative PCR analysis.

Gene	Primer pair	Primer sequence
MBP	Forward	TCACACACGAGAACTACCCATT
	Reverse	TGGTGTTCGAGGTGTCACAA
Olig1	Forward	GGTTTCCGAGCTGGATGTTA
	Reverse	GCGAGCCTGAAAAACAGAAC
Olig2	Forward	AGCAATGGGAGCATTTGAAG
	Reverse	CAGGAAGTTCCAGGGATGAA
PLP	Forward	ACCTGGACCACCTGTCAGTC
	Reverse	GAAAGCATTCCATGGGAGAA
MOG	Forward	GCAGGTCTCTGTAGGCCTTG
	Reverse	CCCTCAGGAAGTGAGGATCA
GalC	Forward	CCACTGGACCAACATGACTG
	Reverse	AGCCATTTGCAAAAATCCAG
NG2	Forward	TCCTGGAGAGAGGTGGAAGA
	Reverse	AAGGATGGTGATCGTGAAGG
Sox10	Forward	GACCAGTACCCTCACCTCCA
	Reverse	GGATGGTCCTTTTTGTGCTG
PDGF-Rα	Forward	TGGCATGATGGTCGATTCTA
	Reverse	CGCTGAGGTGGTAGAAGGAG
CNP	Forward	TTCTGAGACCCTCCGAAAAG
	Reverse	CCTTGGGTTCATCTCCAGAA
GFAP	Forward	CACGAACGAGTCCCTAGAGC
	Reverse	GTAGGTGGCGATCTCGATGT
Nestin	Forward	GATCGCTCAGATCCTGGAAG
	Reverse	AGGTGTCTGCAAGCGAGAGT
TUJ1	Forward	GTCTCTAGCCGCGTGAAGTC
	Reverse	GCAGGTCTGAGTCCCCTACA
PMP22	Forward	TTGCTCTTCGTCTCCACCAT
	Reverse	TGGTGAGAGTGAAGAGCTGG
Periaxin	Forward	GACTCACCGGCAGCTAAGAG
	Reverse	GCCCTTCATCTCGTATCCAG
P0	Forward	AGACTACAGTGACAACGGCA
	Reverse	AGAAGAGCAACAGCAGCAAC

Supplementary Table S3. Oligonucleotides used for reporter plasmid generation.

Oligonucleotide	Sequence
G17	GATCCGGCGCGCCTGCTAGCCTCGAGGGA
G18	CCGGTCCCTCGAGGCTAGCAGGCGCGCCG
G21	TAAAACCGGTCGCCACCATGGTGAGCAAGGGCGAGGAGGATA
G22	TACTTGTACAGCTCGTCCATGCCG
G23	TAAAACCGGTCGCCACCATGGTGAGCAAGGGCGAGGAGGTCA
G52	TATTATCGATGAGCTCCTTCCTGCTTAGGCCG
G53	GCGGGGATCCTAGAATTATTCGAGCTT
G54	CGCGCCACCATGGGCTGTGGCTGCAGCTCACACCCGGAAGATGGA
G55	CCGGTCCATCTTCCGGGTGTGAGCTGCAGCCACAGCCCATGGTGG

Appendix S1: Users' Guide to CEM

This document explains how to use Computer-assisted Evaluation of Myelination (CEM), which was developed by Bilal E. Kerman and Krishnan Padmanabhan under Fred H. Gage's guidance at the Salk Institute in La Jolla, CA, USA. The ImageJ code is written by B.E.K. and MATLAB code is written by K.P. CEM is provided as part of the fair use license. Please reference Kerman et al. (submitted).

CEM is dedicated to the loving memories of Cem and Dilay Kerman, who were taken from us far too early.

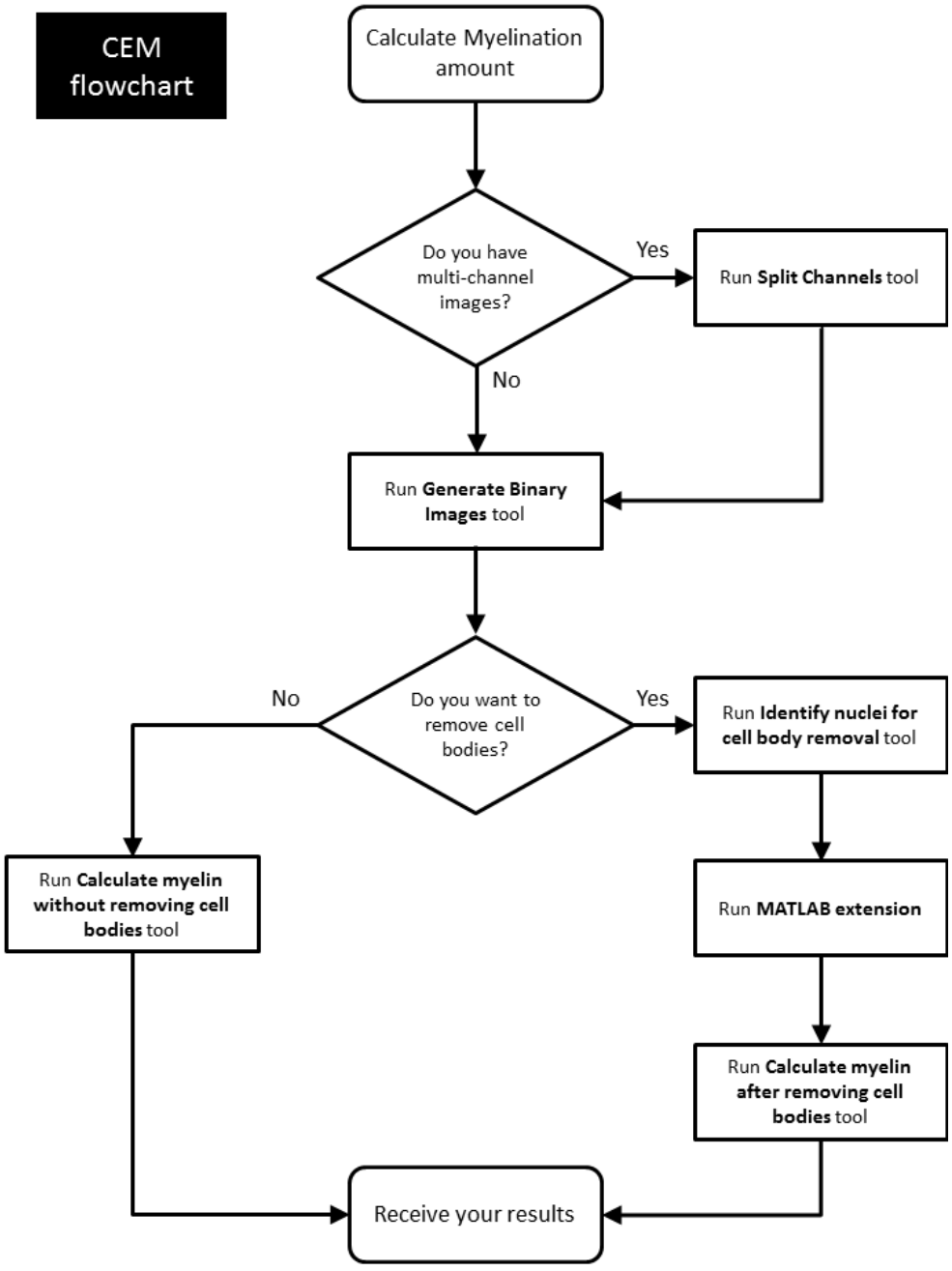

You need an ImageJ version 1.47i or higher to use the calculator. If you want to use the "remove cell bodies" function, you need to run the accompanying MATLAB Toolbox that was tested on MATLAB 2012b. The flowchart above gives a quick look at how the calculator operates and can be used as a quick reference while running it.

How to RUN?

You can run CEM either by first copying the file under the ImageJ plugins folder and starting it from the menu, as seen in the figure below, or by directly opening the "CEM.ijm" file in ImageJ and select "RUN" in the menu option. MATLAB Toolbox can be run by opening the file in MATLAB (see below). If you are processing large image files (>500mb), we recommend a computer with a fast hard-drive for quicker read and write times.

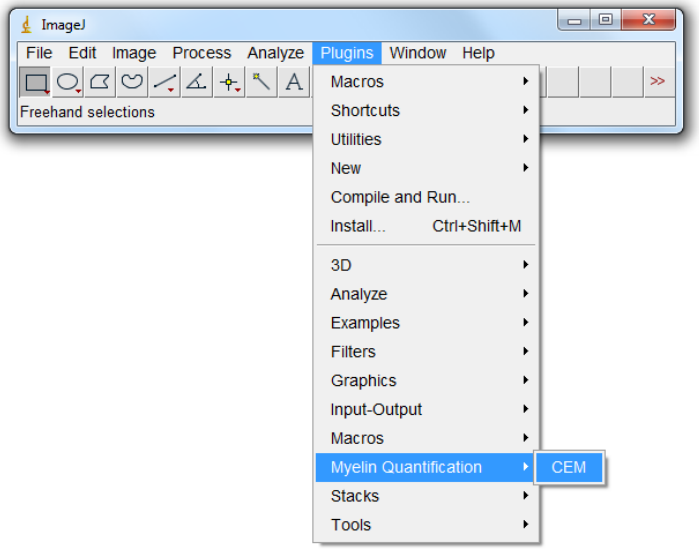

The main menu:

When you start CEM, you will be greeted by a welcome screen. Then you'll get to the main menu. Here you can check on the operation you want to perform.

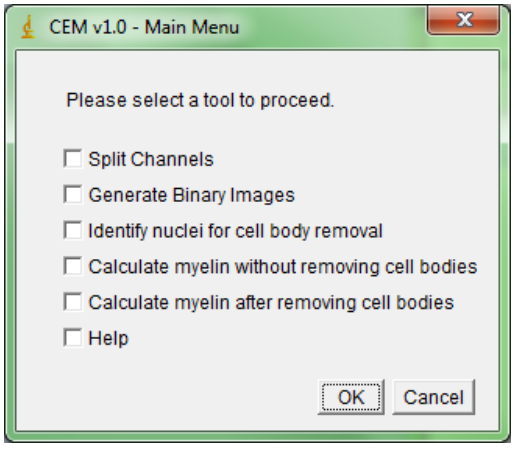

Split channels:

If your images are multi-channel images such as lsm files, composite Tiffs or RGB files, you have to split them into single channel images. The 'Split Channels' tool is designed for that purpose. It will accept any RGB or composite file that ImageJ can open and will ask you to save the new images.

Generate binary images:

The latter calculations are performed on binary images only. This tool will take your single channel images and convert them into binary. As seen in the figure below, you will be asked to adjust brightness by setting minimum and maximum values for your image and select a reference slice. It is crucial that you set brightness to maximize signal-to-noise ratio (1) and press “Apply” (2). If you have image stacks, you need to bring your stack to the reference slice before pressing “OK.” The reference slice is used by the ImageJ binary conversion algorithm to determine values for the rest of the stack. Therefore, it is crucial to select a slice with a large amount of positive signal and low background noise. We suggest that you try a few different settings until you identify the optimum ones and that you record your settings.

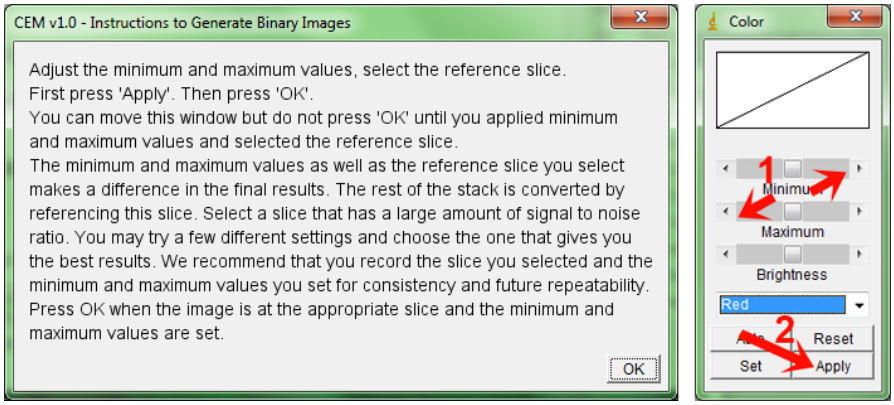

Identify nuclei for cell body removal:

This tool helps you to remove overlap signal associated with the cell bodies. This is a two-step process. First, you need to find the nuclei of the cells you are interested in using this tool. The input files are binary images of oligodendrocytes and/or neurons and nuclei (outputs of “Generate Binary Images” tool or generated by other sources). The first window will ask you to enter an “Identifier” that is used for naming your images and to make a selection as seen in the figure below. The “Identifier” can be any combination of letters, numbers and symbols that are allowed in a file name such as “Exp1-Image1.”

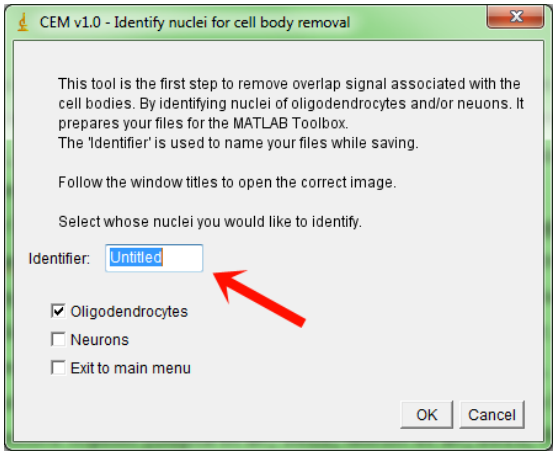

Next you will be asked to choose the image to open. Please follow the window labels to open the correct image as seen in the figure below.

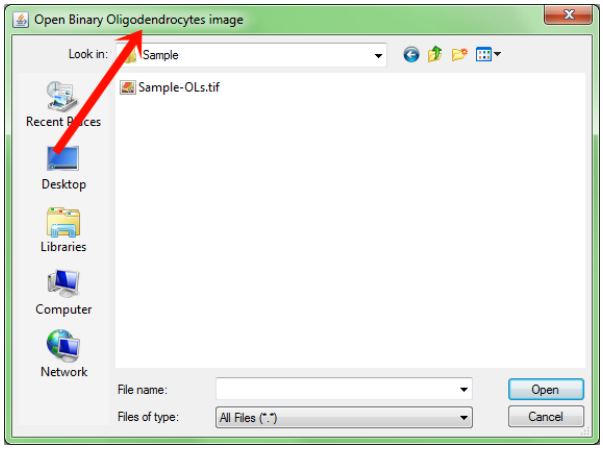

Once the nuclei are identified, the calculator will save the resulting images in a folder that you choose or in the same folder if you just press save.

Second, you need to remove the noise and grow the nuclei into cell bodies using the accompanying MATLAB Toolbox (see below). The application removes particles smaller than a preferred pixel area (for example, 50 pixels square) and grows the remaining nuclei into cell bodies by a preferred number of pixels (for example, 5 pixels).

Calculate myelin without removing cell bodies:

This is the tool where the myelin is identified (as the overlap between axon and oligodendrocyte images) and the results are generated. The input files are binary images of oligodendrocytes and neurons (outputs of “Generate Binary Images” tool or generated by other sources). The first window will ask you to enter an “Identifier” that is used for naming your images (see above) and to select if a subset of axons is different than the others, as seen in the figure below.

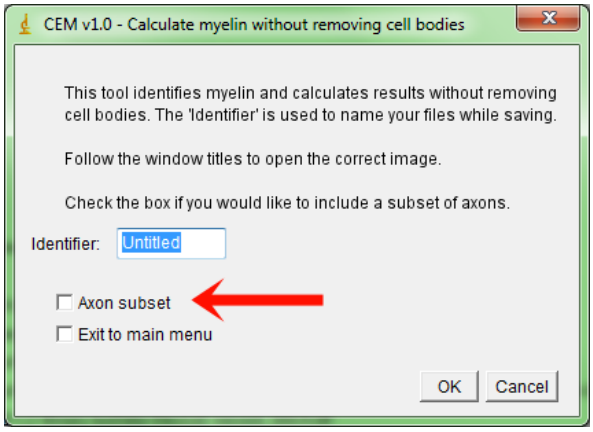

Checking the "Axon subset" option allows you to distinguish some of your axons from the others. For example, a subset of your neurons may be expressing a shRNA to knock down a gene that you suspect affects the myelination of these neurons. As long as the subset of axons is also visually distinct, for example via GFP expression, the calculator will identify both marker-positive and -negative axons. You will need a separate binary image of the distinguishing marker such as GFP.

Next you will be asked to choose the images to open. Please follow the window labels to open the correct images, as explained above.

Once the images are opened, the calculator will start to identify myelin. The myelin is identified as overlap between the oligodendrocyte and axon images by using the AND operator on binary images. The process may take a few minutes, depending on the size of your images and the specifications of your computer. During this process, new images will be generated. When the calculations are complete, the results will be displayed in a new window as seen below, and you will be asked to save the file as a text document. You will also be asked if you want to save the generated images of myelin and subsets of axons. The results are generated as pixel counts and percent values. The pixels are counted using the "Histogram" function of ImageJ (on maximum intensity projections if images are stacks).

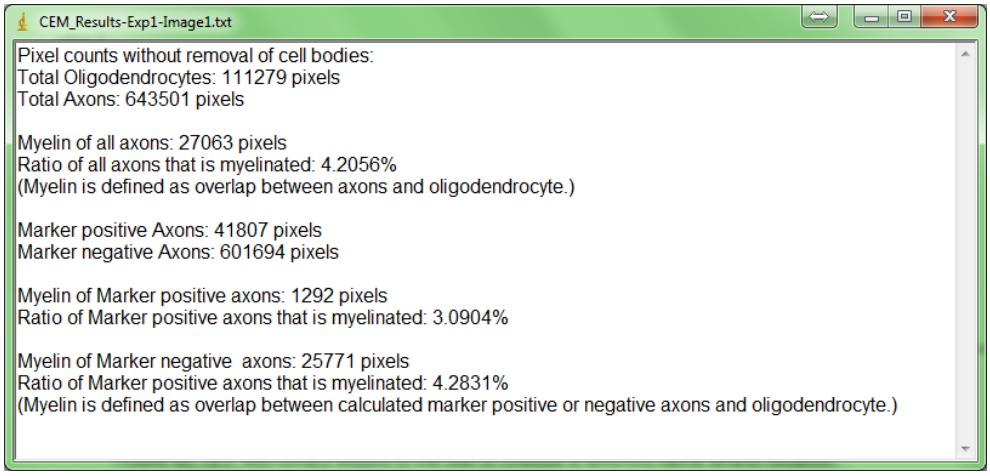

Calculate myelin after removing cell bodies:

This tool is practically the same as the "Calculate myelin without removing cell bodies" tool but removes the cell bodies before identifying myelin. The input files are binary images of oligodendrocytes and neurons (outputs of "Generate Binary Images" tool or generated by other sources) and cell body images as the combined output of "Identify nuclei for cell body removal" and MATLAB Toolbox.

The "Identifier" and "Axons subset" work as described above. You need to check if you want to remove cell bodies from oligodendrocytes and/or neurons. Do not forget to follow the window labels to open the correct image. The output is the same as "Calculate myelin without removing cell bodies" but "CBR" will be added to the titles of any output files to distinguish them.

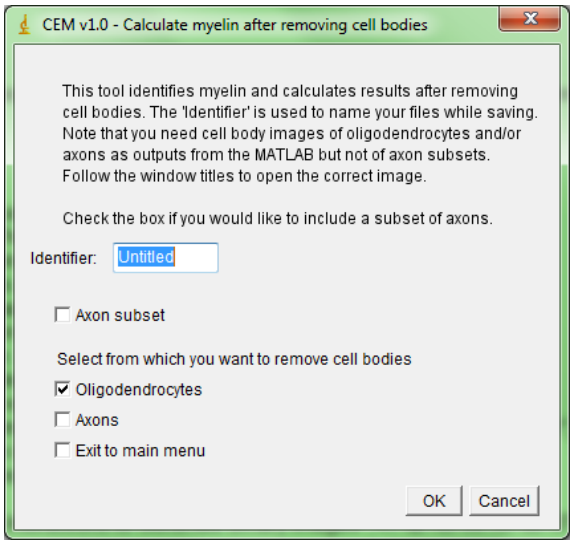

MATLAB Toolbox Installation and Setup:

The MATLAB CEM Toolbox was developed in MATLAB Version R2013a is the OS X 10.9.4 and has been tested on a Windows 7 computer in MATLAB Version R2012b. **NOTE: The INSTALLATION AND SETUP needs to be done ONLY ONCE when the application is FIRST installed on a COMPUTER. After setting up the software, the user can jump to the instructions for running the application.**

Following download of the CEM package, all files should be copied to a directory of the user's choosing. After launching MATLAB, click on Set Path under the Environment.

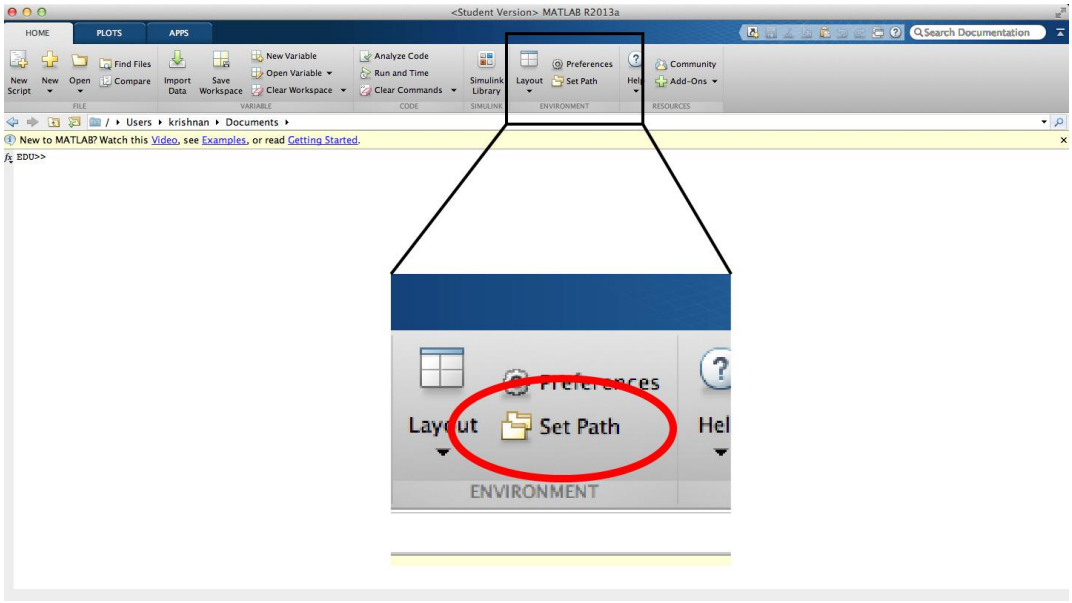

Select Add with subfolders and choose the folder where the downloaded files were copied. Following this, select SAVE and the CLOSE.

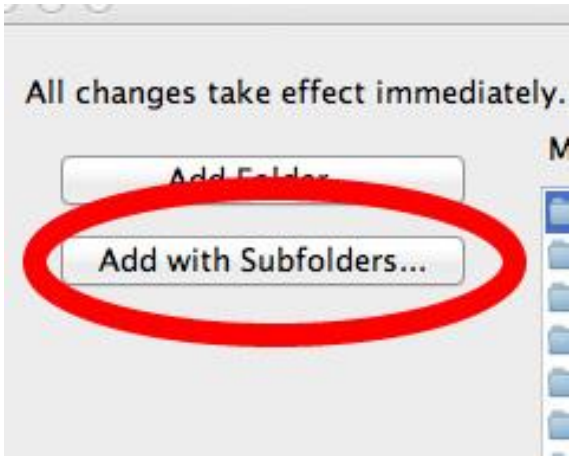

MATLAB toolbox processing:

Following installation, CEM is launched by typing CEM_ToolBOX_v1_1 in the command line of MATLAB.

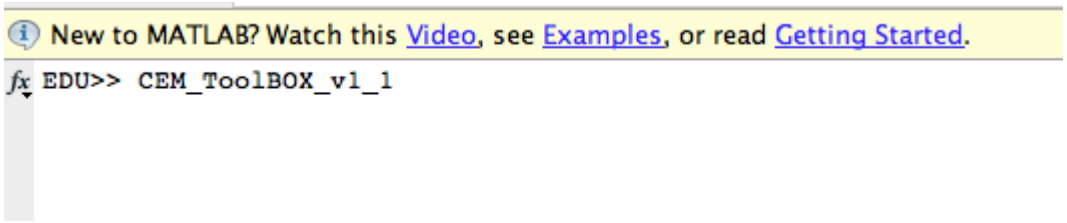

This toolbox allows the user to perform the exclude and dilate functions described in the manuscript. First, a file is loaded by clicking on the LOAD button. The CEM toolbox processes the following file formats (RGB tif, grayscale tif, grayscale tif stack, RGB and grayscale jpeg). Once the file has loaded, it will appear as an image in the image window, and

the VIEW original toggle box will be checked. If the file is a grayscale image or RGB image, it will appear as such. If the file is a tif stack, it will appear as a maximum intensity Z projection in the viewer.

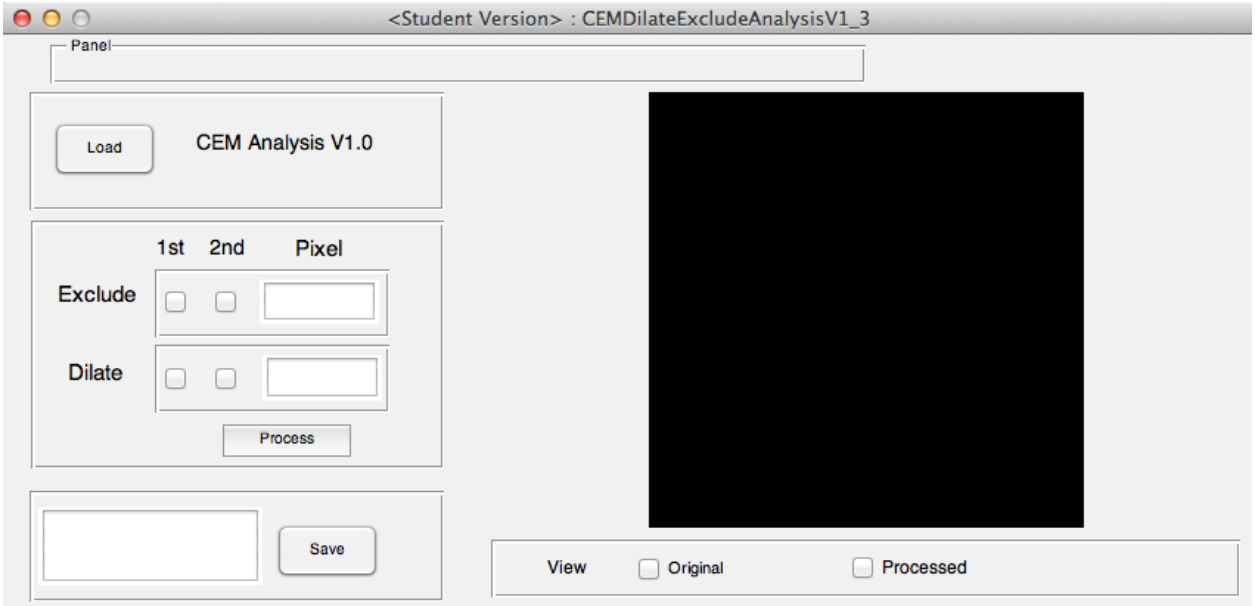

The user has the ability to select different combinations of operations include, exclude only, dilate one, exclude first, then dilate, dilate first, then exclude. This can be done so by toggling between the different conditions in the process toolbox on the left.

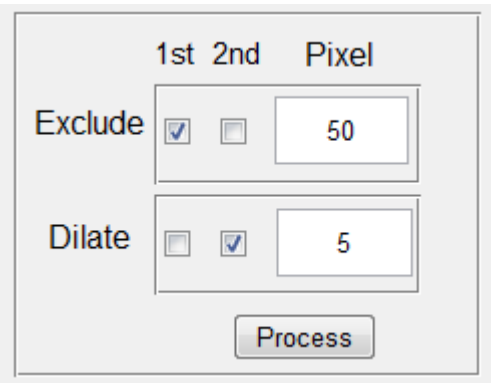

In the example above, CEM will perform object exclusion on the image first and then dilate the image. In this case, the algorithm will exclude objects less than 50 pixels in size, and then dilate the resultant image 5 pixels. This allows for maximum flexibility of parameters for processing. Once the desired operations are selected, click PROCESS.

Depending on the size of the image, this may take some time (and a status bar will note this). Once complete, the image will be displayed in the image window, and the VIEW Toggle box will shift to Processed. The user can toggle between the two images by selecting the Original or Processed toggle box. If a change in the processing parameters is desired, this can be achieved, and the PROCESS button should be clicked. The code will only save the most recent Processed Image.

Once the desired parameters are achieved, and the user is happy with the processing, the image can be saved by selecting the SAVE button. **IMAGES WILL NOT BE SAVED UNLESS THE SAVE BUTTON IS EXPLICITLY CLICKED.** The user may select a name for the file to be saved as (the format the file will be saved is a tif or tif stack, matching the format of the original image). If no file name is entered in the save text box, then a default file name will be used modifying the original file name with the addition of _Processed in the name.

MATLAB Toolbox Exiting and Quitting:

BEFORE QUITTING, ENSURE THAT IMAGES ARE SAVED, AS THIS IS NOT DONE UNLESS THE SAVE BUTTON IS EXPLICITLY CLICKED. The user may quit the program by simply closing MATLAB.

Click here to Download Appendix S2-CEM package

SUPPLEMENTARY MOVIES

Movie 1: An oligodendrocyte wrapping axons monitored in real time for almost eight days. Arrows point to anchor points and oligodendrocyte processes in the course of wrapping. Images were taken every 10 min and are shown here at 12 frames per second. Each frame is a maximum intensity projection of 1 µm apart optical sections. Time is shown as hours:minutes.

Movie 2: A single wrapping event was monitored in real time focusing on the oligodendrocyte processes. The oligodendrocyte sending out the processes is out of the frame at the top. Images were taken every 10 min and are shown here at 12 frames per second. Each frame is a maximum intensity projection of 1 µm apart optical sections. Time is shown as hours:minutes.

Movie 3: 3D reconstruction of serial EM sections were animated to visualize the wrapping from every angle.

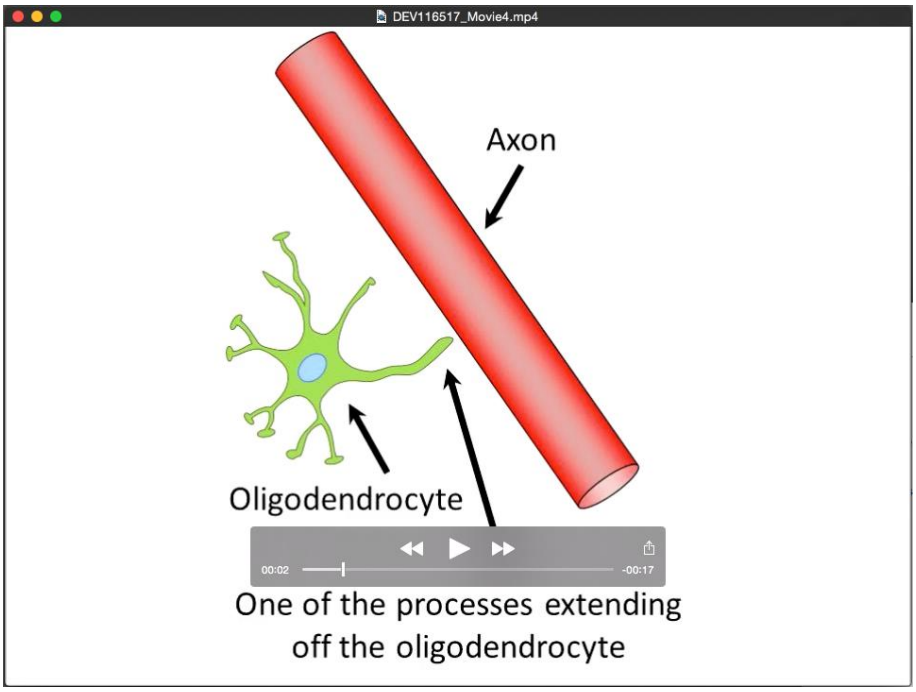

Movie 4: An animation of SARAPE model of myelination.